THE EFFECTS OF SURFACE ROUGHNESS AND STRESS ON LATTICE GAS MODELS USING KINETIC MONTE CARLO MODELING

by
Daniel N. Bentz

A Dissertation Submitted to the Faculty of the
DEPARTMENT OF MATERIAL SCIENCE AND ENGINEERING
In Partial Fulfillment of the Requirements
For the Degree of
DOCTOR OF PHILOSOPHY
In the Graduate College
THE UNIVERSITY OF ARIZONA

2003

THE UNIVERSITY OF ARIZONA ®
GRADUATE COLLEGE

As members of the Final Examination Committee, we certify that we have read the dissertation prepared by Daniel Nabil Bentz entitled The Effects of Surface Roughness and Stress on Lattice Gas Models Using Kinetic Monte Carlo Modeling

and recommend that it be accepted as fulfilling the dissertation requirement for the Degree of Doctor of Philosophy

Kenneth A. Jackson	4/16/03 Date
Joseph H. Simmons	4/16/03 Date
Brian J. Zelinski	4/16/03 Date
William S. Bickel	April 16/03 Date
Srinivas Manne	4/16/03 Date

Final approval and acceptance of this dissertation is contingent upon the candidate's submission of the final copy of the dissertation to the Graduate College.

I hereby certify that I have read this dissertation prepared under my direction and recommend that it be accepted as fulfilling the dissertation requirement.

Dissertation Director Kenneth A. Jackson — July 29, 2003 Date

STATEMENT BY AUTHOR

This dissertation has been submitted in partial fulfillment of requirements for an advanced degree at The University of Arizona and is deposited in the University Library to be made available to borrowers under rules of the Library.

Brief quotations from this dissertation are allowable without special permission, provided that accurate acknowledgment of source is made. Requests for permission for extended quotation from or reproduction of this manuscript in whole or in part may be granted by the copyright holder.

SIGNED: 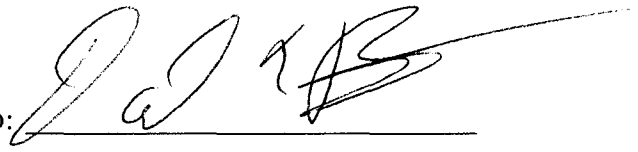

ACKNOWLEDGMENTS

I owe so many people for their help and support throughout the graduate school experience. I would like to give my deepest apologies if I leave anyone out. Foremost, I want to thank Dr. Jackson, whose assistance and encouragement has truly made this document possible. I also want to thank Dr. Nelson who originally inspired my interest in crystal growth. I would like to express my deepest thanks to my Physics cohorts who banded together during my first year at The University of Arizona. To Andrew, Mary, Sharada, and Priya: I don't know how any of us could have managed to survive and remain sane if we hadn't had each other. Special thanks goes to both Andrew and Mary, who on numerous occasions pulled out the dustpan to sweep up my remains. To my parents, grandparents, and close family: I have always been fortunate to have such an encouraging family, who have been much more than a safety net. I would also like to thank the MSE staff who have put up with my many problems; in particular, I would like to thank Valerie who has put up with my wandering around AML trying to clear my head. Last but not least, I would like to thank my girlfriend Heather who has not only put up with me in the last few months of writing but has helped in the proof reading of this document.

I would also like to thank both NASA and the NSF for their financial support of these projects. The support for the surface roughening and eutectic studies work was provided by NASA through grant number NAG8-1667, while the chemical mechanical polishing projects were conducted in conjunction with the NSF KDI project under Grant number 9980015.

DEDICATION

This thesis is dedicated to my grandfather, Louis Bentz, who passed away after my first year of graduate school. It is his work ethic and dedication to family that has made document possible.

TABLE OF CONTENTS

TABLE OF CONTENTS—*Continued*

LIST OF FIGURES

LIST OF TABLES

ABSTRACT

This thesis reports kinetic Monte Carlo computer simulations using a lattice gas model conducted on a variety of systems. These studies may be divided into two main categories: rod eutectics and related surface roughening, and surface morphology changes due to local stresses.

The first grouping is a study of irregular rod eutectic systems. Simulations of directional solidification of rod eutectic systems were conducted using a model similar to the spin one Ising model. Growth of the rods was initiated from columns of pure A atoms embedded in a matrix of B atoms. The growth characteristics of the eutectic depend on the location of the surface roughening transition for the two phases. The surface roughening transition was determined using fluctuation dissipation theory, where the kinetic behavior of the interface is related to a characteristic time of fluctuations about an equilibrium position. These times were determined by time correlations. Results show a sharp transition in the kinetic behavior of the interface as a function of Jackson's alpha factor. This is the first time this method has been used to locate the surface roughening transition. An applied temperature gradient supplied the restoring force for the interface. The roughening behavior of binary alloys was also examined and compared to pure component systems.

The second set of simulations reported here examine the effects of local stress on surface morphology. The weakening of bonds due to the dislocation stress field was studied as the origin of the formation of etch-pits at dislocations. Atoms from a diamond cubic lattice were irreversibly removed with a probability which depends on an local surface configuration as well as on the local stress developed from its physical location with respect to a dislocation in the lattice. In accordance with experimental observations, both faceted and non-faceted dislocation etch-pits have been observed. Simulations of crystal surfaces near equilibrium have reproduced direct experimental results using atomic force microscopy (AFM). The probe tip interacts with the shape and the motion of step edges, and the motion

of a step is retarded in the vicinity of the tip.

CHAPTER 1

KINETIC MONTE CARLO

1.1 Introduction

Computer modeling has had a considerable influence on the present day understanding of the fundamentals of materials science. The computer has provided a platform to characterize the impact of the physical effects on materials processing. Kinetic Monte Carlo (kMC) is a simple and powerful atomistic simulation tool capable of examining the evolution of the solid surface. It uses time scales orders magnitude larger than molecular dynamics simulations, while maintaining the features of a quantized system which are lost in continuum models. This document details the use of kMC simulations of lattice gas models as applied to two distinct projects. The first of these projects is an examination of crystal growth kinetics focusing on irregular rod eutectic systems. The main objective of this project is to examine the growth characteristics of directionally solidified irregular rod eutectics. Motivated by questions in chemical mechanical polishing, the second project's objective is to examine the effects of an imposed stress field on crystal growth and dissolution. While both of these projects are motivated by distinctly different areas, they both benefit from the same simulation tool. Each of these projects have a few sub-projects which are discussed in detail in each of the chapters in this document. KMC simulations have made a considerable impact on the understanding of the solid surface. This includes both growth and dissolution kinetics of both rough and smooth surfaces.

Due to their discreet nature, lattice gas models like kMC appropriately model the anisotropies of the surface energies which have a varying amount of influence on the growth kinetics. This is of particular importance to the surface roughening transition, which distinguishes between rough and smooth interfaces [71]. Surface roughening studies have been conducted on both simple cubic (SC) systems [71, 98] and on diamond cubic lattices [33]

using solid on solid (SOS) models. Lattice gas models were used to model the screw dislocation spirals [38, 103], which are the predominate growth mode in surfaces below the surface roughening transition. Other studies have examined the effects of step density on the surface energy [70, 95, 98]. Dissolution of surfaces using focusing on both diamond cubic and simple cubic systems [101, 96]. Lastly, one of the largest contributions of kMC has been the understanding the non-equilibrium segregation effects [37, 55]. By using the Jackson, Gilmer, Temkin (JGT) model of interface kinetics, kMC was used to relate the direction dependence of the non-equilibrium segregation coefficient to the growth rate of the interface and the diffusion of dopants in the liquid.

The ultimate goal of the crystal growth kinetic projects is to understand, and later control, the micro-structure of directionally solidified irregular rod eutectics. In these systems, two solid phases are grown from a single liquid phase in which the micro-structure strongly depends on the growth rate. This self-assembled micro-structure is typically developed on the micron to sub-micron length scales and can have a significant impact on the electronic, optical, and mechanical properties of the composite systems. The regular rod eutectic system was examined using a JGT model treatment of a binary alloy system to verify that growth followed the Jackson-Hunt model. Direct application of this method to irregular eutectics directly lead to two separate projects. These are classifying the roughening behavior of a binary alloy and determining the surface roughening transition of a pure face centered cubic (FCC) system.

The second project discussed in this document focuses on understanding the primary contributors to chemical mechanical polishing. While it is widely used in semiconductor processing, much of our current understanding of the interactions between chemical attack and physical abrasion are not understood. In chemical mechanical polishing, the combined effects of chemical attack and mechanical stress are orders of magnitude greater than either acting alone. This work has focused on two distinct systems: dislocation etch-pitting and the impact of local stress fields on the growing step edge. Both these projects use simulations based on a spin 1/2 Ising model of the liquid-solid interface. Bond energies in the

solid have a geometric perturbation to represent strain in the solid.

This first chapter provides an overview of crystal interface kinetics and motivate the use of kMC as a simulation technique. The JGT interface model and relationship to the spin Ising model systems is discussed in relation to solid-liquid interface. Next, the computational model with a small explanation the algorithm will be introduced. Finally, an overview of the projects included in this dissertation will be presented with a brief statement of their individual importance.

1.2 Solid Interface Kinetics

When the crystallization rate depends on the mobility of the atoms in the liquid, the rate at which atoms join and leave the solid depends on their corresponding activation energies. This growth model is typically referred to as the Wilson-Frenkel growth model [99] which is representative of many rough solid-liquid systems, including silicon's $\{100\}$ surface. While the Wilson-Frenkel model describes rough interfaces, the rate equation developed here may be used describe both rough and smooth interfaces. This particular derivation was conducted by Jackson [57].

This derivation is started by defining the activation energy for a liquid atom to join the solid is the difference of the thermal energy of the average liquid atom at the interface(E_T) and the energy of an atom in the solid(E_S). Thus, the rate liquid joins the solid may be written as

$$R^+ = R_o^+ exp\left(-\frac{E_T - E_S}{k_B T}\right) = R_o^+ exp\left(\frac{-Q}{k_B T}\right) \tag{1.1}$$

Similarly, the activation energy for an atom to go from the solid to the liquid may be written as

$$R^- = R_o^- exp\left(-\frac{(E_T - E_L)}{k_B T}\right) = R_o^- exp\left(\frac{-(Q+L)}{k_B T}\right) \tag{1.2}$$

where E_L is the energy of an atom in the liquid phase. By defining Q as $E_T - E_S$ equations 1.1 and 1.2 may be written in terms of the latent heat, L, or the difference in the

enthalpies E_L and E_S of the two phases. Both R_o^+ and R_o^- are pre-exponential factors which depend on the hopping rate and the concentration of arriving and departing atoms at the interface.

At equilibrium, the arrival and the departure rates are equal to each other the expression for R_o^+ and R_o^- may be written as

$$\frac{R_o^+}{R_o^-} = exp\left(-\frac{L}{k_B T_m}\right) \tag{1.3}$$

where T_m is the melting temperature of the system. By substituting equation 1.3 into equations 1.1 and 1.2 we get

$$R^+ = R_o\, exp\left(-\frac{L}{k_B T_m}\right) = R_o\, exp\left(-\frac{\Delta S}{k_B}\right) \tag{1.4}$$

$$R^- = R_o\, exp\left(-\frac{L}{k_B T}\right) \tag{1.5}$$

where

$$R_o = R_o^-\, exp\left(-\frac{Q}{k_B T}\right) \tag{1.6}$$

Equation 1.4 may also be written in terms the entropy difference between the two phases since $\Delta S = \frac{L}{T_m}$. An expression for the velocity of the interface is then given by the difference between the rates which atoms join and leave the solid

$$V = a\left(R^+ - R^-\right) = a\, R^+\left(1 - exp\left(-\frac{L\Delta T}{k_B T_m T}\right)\right) \approx a\, R^+ \frac{L\Delta T}{k_B T_m T} \tag{1.7}$$

where $\Delta T = T_m - T$ or the under-cooling of the interface and a is the square root of the atomic volume. Thus, for small under-coolings ($\Delta T \ll T_m$), the interface face velocity is linear with under-cooling.

To relate the diffusion coefficient to the growth rate coefficient, R_o, in equation 1.6, it is beneficial to rewrite equation 1.4 in terms of an add-atom arrival rate at a repeatable step site, ν^+.

$$\nu^+ = \nu_o\, exp\left(-\frac{Q}{k_B T}\right)\, exp\left(-\frac{L}{k_B T_m}\right) \tag{1.8}$$

The pre-exponential factor, ν_o, is just the Debye frequency.

The diffusion coefficient, D, is then related to ν_o through equation 1.9 where Λ is the characteristic diffusion length in the liquid.

$$D = \frac{1}{6}\Lambda^2 \nu_o \, exp\left(-\frac{Q}{k_B T}\right) \tag{1.9}$$

The velocity of the interface may then be written in terms of the cube root of the atomic volume, a, and the fraction of surface lattice site density which are repeatable step sites, f. Thus, the velocity of the interface may be written as

$$V = \frac{6aD}{\Lambda^2} uf \tag{1.10}$$

where u is

$$u = 1 - exp\left(\frac{L\Delta T}{k_B T_m T}\right) \tag{1.11}$$

Similar models have been applied to binary systems by including the diffusion of the second species [52]. In both cases surface morphology plays a significant role in growth kinetics, since there is no analytical solution for density of repeatable step cites.

Alternatively, the solidification rate may be independent of diffusion in the liquid. This is the case observed in molecular dynamic simulations with Lennard-Jones [13] interactions. This model is representative of systems where solidifying species have a high amount of symmetry and low entropies of fusion, as with many metals. In this system, the rate at which atoms join the solid depends on thermal velocity of atoms in the liquid is given by:

$$\nu_+ = \frac{1}{\lambda}\sqrt{\frac{3k_B T}{m}} exp\left(-\frac{\Delta S}{k_B}\right) \tag{1.12}$$

This leads to the experimentally confirmed growth rate of

$$V = \frac{a}{\lambda} f \sqrt{\frac{3k_B T}{m}} exp\left(-\frac{\Delta S}{k_B}\right)\left[1 - exp\left(-\frac{\Delta \mu}{k_B T}\right)\right] \tag{1.13}$$

For the purposes of relating this growth rate expression to equation 1.7, the chemical potential difference $\Delta\mu$ may be written as:

$$\Delta\mu = \frac{L\,(T_m - T)}{T_m} \tag{1.14}$$

While the growth rates of these two processes are distinctly different, their surface roughening behavior can be effectively modeled using a lattice gas model. The lattice gas model used in this document has its foundations in the JGT model.

1.2.1 Ising Model Systems

The Ising model system [47] was first developed to explain the magnetic phase transition of materials at the Curie temperature. Since then it has been extensively examined in statistical mechanics in multiple dimensions to understand the behavior of systems about their critical points. Models sharing the same universality class have also been developed to examine surface morphology and interface kinetics. In this model a system of magnetic particles interact with each other by nearest neighbor interactions and with an eternally applied magnetic field. Thus, the Hamiltonian of the system can be written as

$$H = \frac{1}{4}\sum_{(i,j)} \Omega\sigma_i\sigma_j - \sum_i h_i\sigma_i + H_o \tag{1.15}$$

Here Ω is the spin-spin coupling constant, h_i is the strength of the applied magnetic field, and H_o is a constant. The σ_i's represent that spin state the at i-th position in the lattice. In the spin 1/2 system this spin can be up or down (+1/2 or -1/2) while in the spin one systems this can be up down or zero (1, -1 or, 0). The j-th indecency sums over the nearest neighbors of the i-th lattice site.

Ising originally solved this model for the one dimensional case, saw no phase transition, and erroneously deduced that the two and three dimensional systems would display the same behavior. Later, Onsager solved the two dimensional case of the spin one half system [82] and applied these results to a crystal growth model. This crystal growth model was then extended by Burton, Cabrera, and Frank [15].

The application of the spin one Ising model to binary alloy systems has been developed by Gilmer [39, 40]. In such a system the binary solid solution is in contact with a single

liquid phase. The Hamiltonian representing this lattice gas model system can be written as

$$H = -\sum_{(i,j)}\left[C_i^A C_j^A \phi_{AA} + \frac{1}{2}\left(C_i^A C_j^B + C_i^B C_j^A\right)\phi_{AB} + C_i^B C_j^B \phi_{BB}\right] - \sum_i \left(C_i^A \Delta\mu_A + C_I^B \Delta\mu_B\right) \quad (1.16)$$

In this model, each lattice site is occupied by a solid A or B, or a liquid atom. This liquid atom may be A or B as well. However, the distinction of an atom in the liquid phase is purely a fixed probability which depends on the liquids composition. C_i^A and C_i^B are the occupancy of the lattice site i, and are equal to one where the lattice site is an A solid or a B solid respectively. Otherwise their value is zero. The ϕ_{XY}'s in this expression are solid-solid bond energies between atoms X and Y, while the $\Delta\mu_X$ is the difference in the chemical potential of a system of pure liquid and solid X atoms.

This is the spin one Ising model treatment of the solid-liquid interface where each lattice site can exist in one of three states. The Hamiltonians represented in equations 1.15 and 1.16 are representative of the same system. This is apparent with the transformation of

$$\Omega = \frac{\phi_{AA} + \phi_{BB}}{2} - \phi_{AB} \quad (1.17)$$

$$h_i = \frac{1}{2}\left[\Delta\mu_A - \Delta\mu_B\right] - (Z - Z_i)\frac{\phi_{AA} - \phi_{BB}}{4} \quad (1.18)$$

Similarly, single component systems are referred as spin 1/2 systems since each lattice site contains either a solid or liquid atom. While the JGT model, discussed in the next section, deviates from the spin one Ising model system when examining binary alloys, the JGT model shares the same universality class with the spin 1/2 system when dealing with single component systems.

1.2.2 JGT model

The JGT model [3] is a lattice gas model, developed by Jackson, Gilmer, and Temkin [37, 58, 59] and was used to examine kinetics of the two component liquid-solid interface systems. In most cases the kinetics of a binary liquid-solid and liquid-gas systems are governed

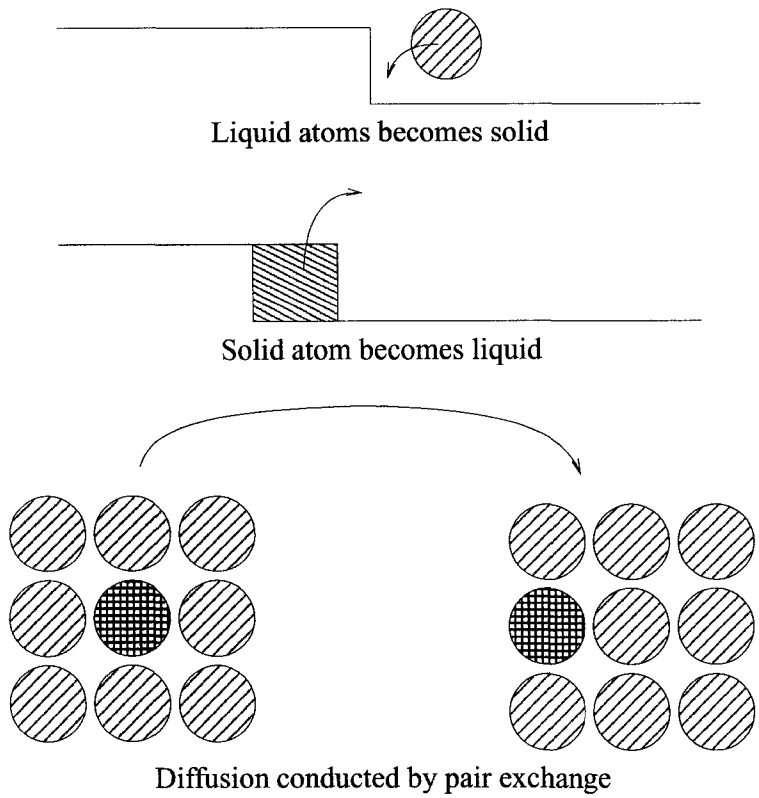

FIGURE 1.1. Simulation Events

by three distinctive rates as shown in figure 1.1. These events are the rate at which atoms arrive to join the solid, the rate at which atoms depart the solid, and the rate heterogeneous diffusion in the liquid, assuming that the diffusion in the solid is inconsequential. These rate equations are compliant with rate equations 1.4 and 1.5 of the previous section.

In the JGT model atoms are added to the solid surface at a rate which depends on the entropy difference between the solid and liquid phases. Equation 1.19 is the analytical expression of this rate.

$$\nu_i^{LS} = \nu_o \, exp\left(-\frac{\Delta S_i}{k_B}\right) exp\left(-\sum_j \frac{\Phi_{ij}}{k_B T}\right) \tag{1.19}$$

Here ΔS_i is the entropy difference between the liquid and the solid phases of the A and

B atoms, and ν_o is the pre-exponential factor with units of 1/time. All simulations reported here are a special case of the JGT model which is closer to the spin one Ising model system. Also, all liquid-solid bond energies are set to zero so that that the last exponential term in equation 1.19 is equal to one. Correspondingly, atoms leave the solid and join the liquid at a rate depends on the configuration of atoms on the solid surface.

$$\nu_i^{SL} = \nu_o \, exp\left(-\sum_j \frac{\Phi_{ij}}{k_B T}\right) \tag{1.20}$$

Both solid-liquid bonds and liquid-liquid bonds energies are set to zero. These agree with the equations 1.4 and 1.5 since $L_\alpha = \frac{Z}{2}\Phi_{AA}$ and $L_\beta = \frac{Z}{2}\Phi_{BB}$ where L_α and L_β are the latent heats of fusion for solids comprised of pure A and pure B respectively.

Diffusion is typically limited to the liquid and is implemented by pair exchange of B atoms at a rate proportional to add-atom arrival.

$$\nu_i^D = \theta \, \nu_i^{LS} = \frac{6\,D}{a} \tag{1.21}$$

Here θ is the proportionality constant. This rate may also be written in terms of the diffusion coefficient D and the cube root of the atomic volume, a. These three rate equations are the foundation of the kMC simulation presented here.

There is a distinct difference between an ideal solution liquid in contact with a regular solution solid, and the spin one Ising model of a binary system. The spin one Ising model treats the liquid as a single entity where the A and B components are uniformly present in the liquid phase. This relatively minor simplification has a significant impact on the kinetics of the interface. Effectively these systems have embedded the entropy of mixing term into the choice of of the concentration field on the solid surface.

1.3 Kinetic Monte Carlo

The underlying simulation method used in this dissertation is kinetic Monte Carlo (kMC) modeling. KMC is a simulation technique which can be used to examine micro-structures

with atomistic resolution on macroscopic times scales. KMC is an event based Monte Carlo (MC) algorithm in which examines large scale morphology using small scale Markovian processes. This is distinctly different than classical MC utilizing a Metropolis algorithm or molecular dynamics (MD) simulation which the development of a Hamiltonian is at the center of the simulation technique. There have been many good reviews of kMC used in crystal growth [41, 103, 66, 54, 97]. Another review presented by Binder examined the general application of Monte Carlo methods and explore the mathematical underpinning of these methods [8]. Binder has also written an introductory text on implementation on a variety of other systems and has included detailed discussions of useful algorithms [9].

In general the term lattice gas refers to a class of models where the simulation space is coarsely discretized and the actions of particles on the grid depends on their local neighbors. In the kinetic Monte Carlo simulations presented here, the lattice is used to model the liquid solid interface, as displayed in figure 1.2. The simulation cell is divided into a grid in which every node on the grid is occupied by either a solid or liquid atom. All of the next nearest neighbor interactions are folded into the nearest neighbor interactions.

The systems develop by choosing and implementing events one at a time based on their probability of occurrence. These events are chosen at random using their weighed probability of occurring. The system develops along a Markovian chain process since the individual choice of an event is not impacted by the past history of that individual location.

1.4 Implementation

The simulations described in this dissertation were all conducted using the same algorithm implemented with the same code. There are two main parts to this implementation: simulation cell lattice development and event management. The implementation of both of these parts takes advantage data structures in the programing language C.

The main purpose of the development of the simulation cell is to record the state of each point on the lattice and to keep track of the nearest neighbors of all lattice sites. The lattice

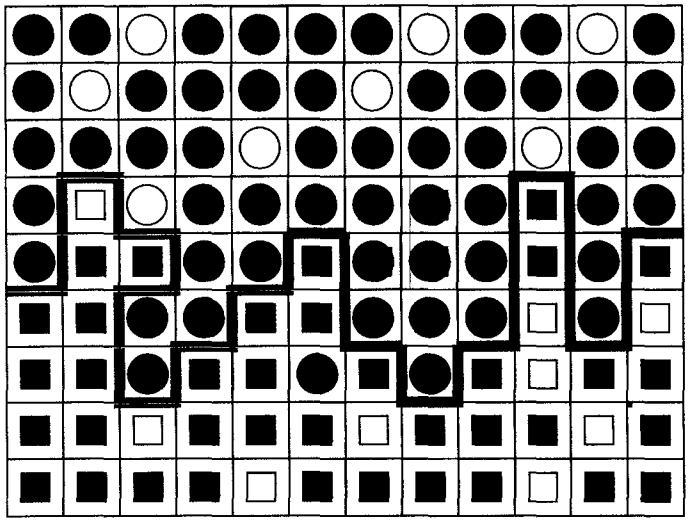

FIGURE 1.2. Simulation Cell

Simulations are conducted by examining nearest neighbor interaction. All lattice sites are occupied by a single atom. In the binary JGT model, atoms can be a solid A or B atoms (white or black squares) or a liquid A or B atom (white or black circles). In the above diagram, the interface is represented by the gray line. In this model A and B atoms are locally conserved. That is, A atoms are allowed to be solid or liquid but not allowed to transform into a B atom.

development code that was used for these simulations reported here was developed by Kirk Beatty [3]. The lattice is developed as a one dimensional array of structures. Each structure holds the type of atom at its lattice site, the list of nearest neighbor of this lattice, and its coordinates in the simulation cell. This is done with lattices with cubic symmetry and initial lattice orientations. Simulations are conducted using periodic boundary conditions.

The kMC algorithm used in these studies is similar to the event driven the BLK algorithm developed by Bortz, Lebowitz, and Kalos [11]. However, the implementation of the algorithm is closer to that proposed by Blue and Beichl [10]. In both, of these algorithms all possible events in the simulation cell are recorded and are chosen at random with a weighted probability of occurring. Once an event is chosen, it is implemented. This is different from a Metropolis algorithm which randomly visits sites on a lattice and may or may not implemented a change depending on the local configuration. The modification that Blue and Bleichl implemented was to increase the speed of finding an event with a binary search tree.

The algorithm employed here records all possible events for a given lattice configuration on the bottom of a balanced binary search tree [67]. Each of these event nodes contains information on the location of the potential event and the probability that that event will occur. Also, each event node has a parent node which contains the sum of the probabilities of its two children. Likewise each parent has a single parent which contains the sum of the probabilities of its two children. This progeny tree continues until there is a single head node which records the sum of the probabilities of all the events in the simulation, Q_{tot}.

$$Q_{tot} = \sum_i \nu_i \tag{1.22}$$

An single event is picked by starting at the top of the tree and successively choosing a number between zero and the value of this node chooses events. If this value is less than the right branch, then right branch becomes the current node until a node representing an event is reached. After an event has been implemented, all events affected by the change are updated, and the clock is advanced by the reciprocal of the head node's frequency. This

implementation time is shown in the following equation.

$$\Delta t = 1/\sum_i \nu_i \tag{1.23}$$

Random numbers are generated using the long period generator Mersenne Twister. [76]

In general, to eliminate non-physical bulk effects, liquid atoms surrounded by liquid atoms are not allowed to become solid, and solid atoms surrounded by solid atoms are not allowed to become liquid. This scheme appears to violate detailed balance, but it does not. Not applying these conditions leads to solid atoms "floating" in the liquid and diffusing by a non-physical solidifying process.

1.5 Application

The remaining chapters in this dissertation motivate and discuss the application of this kMC algorithm to a variety of systems. While developed as five distinct projects, the first three are motivated by the study of irregular eutectic systems, and the last two are motivated by a chemical mechanical polishing study.

1.5.1 Rod Eutectic Simulations

In this section the project of steady state growth of a rod eutectic from the melt is detailed. These simulations used a kinetic Monte Carlo model with diffusion by pair exchange only in the liquid phase. The bond energies were derived from the equilibrium phase diagram. Growth of the rods was initiated from columns of pure A material embedded in an B matrix which were arranged in a close packed formation with periodic boundary conditions. In the kinetic Monte Carlo simulations the growth of each phase was faceted or non-faceted phases depending on the entropy of fusion. Lastly, this chapter discusses the difficulties of simulating irregular eutectic growth, and motivates the projects of the surface roughening behavior of a binary alloy.

1.5.2 Surface Roughening Transition

In this chapter the surface roughening transition of the $\{100\}$ FCC surface using fluctuation dissipation theory. The simulations were conducted using a spin 1/2 Ising model treatment of the solid-liquid interface with simulation cells 50 by 50 by 10 lattice units in size. These interfaces were studied at equilibrium with an imposed temperature gradient to supply a restoring force for the interface. Fluctuations in the number of solid atoms in the system about the equilibrium position were examined using time correlations. These characteristic times were then used to calculate the kinetic coefficient of the system. A dramatic change in these characteristic times which locate the surface roughening transition has been observed.

1.5.3 Surfaces Roughness of Binary Alloy and Irregular Rod Eutectics

Although the surface roughening transition in single component systems has been studied extensively, the surface roughening transition in binary alloys has not. The surface roughness, which is defined as the density of lateral unsatisfied bonds at the interface has been determined for both the pure components and for alloys of various compositions. The surface roughness for a pure material depends on the change in bond energy associated with the transformation, divided by the melting point. Using systems where the solid phase contains essentially one component, this project examined the surface roughness of the alloy systems. It was shown that the surface roughening behavior depends on the value of the Jackson α-factor when liquidus temperature of the alloy is used as the melting point of the system. This chapter then applies the knowledge of the surface roughening behavior of binary alloy systems and the surface roughening transition to re-examine the irregular rod eutectic system.

1.5.4 Dislocation Etch-Pit

Chemical mechanical polishing and stress corrosion cracking result from chemical attack at stressed regions. To better understand the combined effects of chemical attack and stress,

a kinetic Monte Carlo (kMC) study of the formation of dislocation etch-pits was pursued. In the simulations, atoms from a diamond cubic lattice were irreversibly removed with a probability that depended on an atom's number of nearest neighbors as well the local stresses. These stresses are imposed on the simulation by adding an energy term which is dependent on an atom's physical location with respect to a dislocation. In accordance with experimental observations, both faceted and non-faceted dislocation etch-pits have been observed. Simulations were performed for various values of the strength to the etchant as well as the magnitude of the stress produced by the dislocation.

1.5.5 Stressed Step Edge

Studies of crystal surfaces at near equilibrium conditions using atomic force microscopy (AFM) have demonstrated that the probe tip interacts with the shape and the motion of step edges. A step edge is found to retract near the probe tip, and the motion of the step is retarded in the vicinity of the tip. This effect, which is limited to within a few atom diameters of the tip, has been attributed to stresses in the crystal caused by the proximity of the tip. The stress field from the probe tip was introduced as a cylindrically symmetric Gaussian energy field which was incorporated in a kMC model. Steps on the surface were generated by offsetting the periodic boundary conditions. The local morphology of the step was found to depend on the strength and size of the stress field, as well as on the kink site density of the step. The magnitude of the energy field which was sufficient to significantly alter the shape of the step was only a few percent of the bond energy. These results suggest a novel explanation of the enhanced material removal, which is the basis of chemical mechanical polishing.

CHAPTER 2

ROD EUTECTIC SIMULATIONS

2.1 Introduction

There has been considerable interest in directionally solidified eutectic systems for many years [43, 68, 44]. Much of this interest is due to their self-assembled microstructures. Eutectic systems are comprised of two solid phases in contact with a single liquid phase. When these systems are directionally solidified, the two phases self assemble with microstructures which depend on the solid phases' volume fraction. These structures may be laminae or rods whose characteristic size and uniformity depend on the solidification conditions. The formation of these microstructures has a dramatic impact on the mechanical, electrical, and optical properties of these materials.

The distinction between regular and irregular eutectic systems is based on the surface roughness of the two solid-liquid interfaces. While both of the solid-liquid interfaces of the regular eutectic are rough, above the surface roughening transition, one or both of the irregular eutectics's interfaces are smooth, or below the surface roughening transition. This distinction is important since the directional solidification of regular eutectic systems are relatively well understood and closely follow the Jackson-Hunt model [60, 45] (J-H model). However, this is not the case with irregular eutectic systems since surface nucleation complicates the growth kinetics. These irregular eutectics typically grow with a larger inter-phase spacing and with a non-uniform micro-structure. There have been a few models which have explored the impact of relaxing assumptions on the J-H model; however, none of these have examined the growth kinetics of a coupled rough smooth interface.

The goal of the rod eutectic project is to understand the growth kinetics of irregular eutectic alloys. In particular, this project was motivated by the need to control the uniformity of the mircostructure of irregular eutectics such as Ge-$TiGe_2$ and Si-$TaSi_2$ and

provide a modeling tool which could be used to ascertain the impact of gravity on this system. Here, control of the inter-rod spacing, which impacts the density and geometry of the metal-semiconductor junctions, is critical in controlling the electronic properties used in the applications to high voltage transistors and high quantum efficiency photodiodes [28, 29, 89, 80]. Since the JGT model appropriately models the interface kinetics of a regular solution solid in contact with a ideal solution liquid above and below the surface roughening transition, it is a clear choice in modeling this system. The JGT model is implemented on an eutectic system constructed with two solid phases rich in either A or B atoms. Thus, with the JGT model, irregular systems may be as easily studied as regular systems. This statement, while completely true, does contain some significant difficulties which will be explored. Many of these results have been previously published in the proceeding to the NASA 2002 Materials Science Conference [4].

2.2 Background

Eutectic systems are comprised of a mixture of two (or more) types of species. These exist as mixtures of a single phase liquid at temperatures above the melting of the system and form solids of two types of phases at lower temperatures for a range of compositions. The melting point of the system is lower than that of its pure constituents. This is best described in figure 2.1. While the solid phases are also mixtures of the two types of species, they are individually rich in one of the two. In the sample phase diagram, these individual species are denoted as A and B.

For this project we have focused on directionally solidified eutectic structures in which there is a single solid-liquid interface. The use of the phase eutectic systems not only refers to the phase diagram shown in figure 2.1, but also refers to the solid-solid structure developed when systems are solidified near the eutectic composition. In this system the A constituents in the liquid diffuse to join the A-rich alpha phase while the B constituents diffuse to join the B-rich beta phase. There are two types of structures which these phases

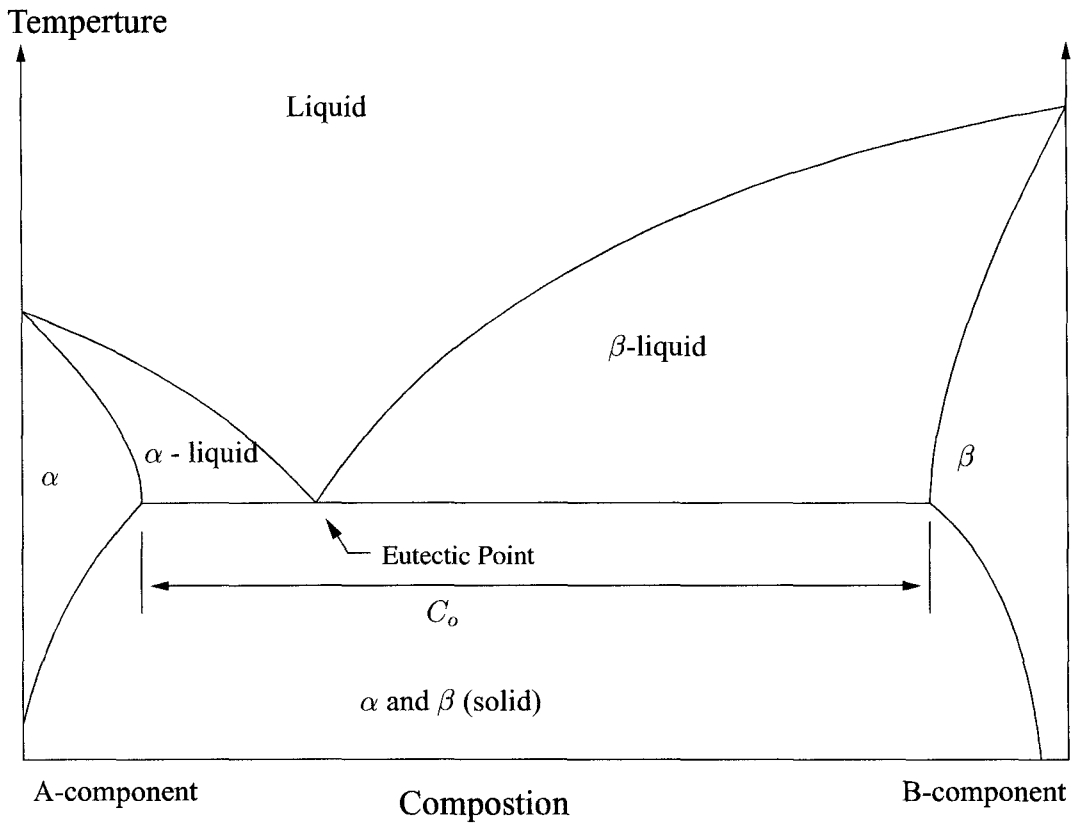

FIGURE 2.1. Example Eutectic Phase Diagram

Eutectic phase diagram displays both the liquidus and solidus of the α and β phases. The eutectic point denotes the temperature and composition of the liquid of the system when all three phases are in thermal equilibrium with each other.

can order, a laminar structure and a rod structure. The solid phase forms a laminar structure if the two solid phase have roughly the same volume fraction the solid phase. However, if one of the two phases dominates, the minor phase will form rods in the major phase. This rod structure is energetically favorable if the volume fraction of the minor phase is below $\frac{1}{\pi}$.

Directional solidification of eutectic systems does not have too occur at the eutectic composition; instead systems may still solidify off eutectic composition by eutectic growth modes [46, 14]. The extent of the eutectic growth mode depends on the competing growth modes of the dendrites of either the two components. The interface kinetics is governed by the fastest of these modes.

2.2.1 Jackson-Hunt

In 1966 Jackson and Hunt presented a model for the directional solidification of both the laminar and rod eutectic systems [60, 45]. This was done by examining the concentration of the two components of the two phases in the liquid phase as the two species diffuse to the two solid phases. Using this composition profile of the liquid in conjunction with the solid's interface curvature, the under-cooling of the interface was calculated. As a result of this derivation, relationships between interface under-cooling ($\Delta T = T_E - T$), solidification rates (v), and characteristic rod or laminar spacing (R) were developed. These relationships were in terms of the thermodynamic properties of the system. This discussion will only present results for rod eutectic systems.

$$\Delta T\, R = 2\, m\, a^R \tag{2.1}$$

$$R^2\, V = \frac{a^R}{Q^R} \tag{2.2}$$

$$\frac{\Delta T^2}{V} = 4m^2\, a^R Q^R \tag{2.3}$$

Here T_E is the eutectic temperature, the temperature where all three phases are in thermal equilibrium. In these relationships, m is a parameter which depends on the slopes of the liquidus lines of the α and β phases, m_α and m_β at the eutectic point.

$$\frac{1}{m} = \frac{1}{m_\alpha} + \frac{1}{m_\beta} \tag{2.4}$$

The coefficient a^R is based on the parameter a in the the Gibbs-Thompson relationship

$$\Delta T = m\left[C_E - C(x)\right] + \frac{a}{r(x)} \tag{2.5}$$

which relates the effect of local curvature, $r(x)$, to the under-cooling of the interface. In this relationship, C_E is the eutectic composition, and $C(x)$ is the composition at a point x along the interface. The Gibbs-Thompson parameters of interest here are a_α and a_β which are the values from the alpha-liquid and beta-liquid interfaces respectively. In particular, a^R is related the parameters a_α and a_β, as well as ζ, the ratio of the volumes of the two solid phases, and the slopes of the liquidus lines m_α and m_β.

$$a^R = 2\sqrt{1+\zeta}\left(\frac{a_\alpha}{m_\alpha} + \frac{a_\beta}{\zeta m_\beta}\right) \tag{2.6}$$

Here ζ is the ratio of the volume fraction of the major phase to that of the minor phase.

The parameters a_α and a_β depend on the thermodynamic properties of latent heat (L), eutectic temperature(T_E), interfacial free energy (σ), and the angle of the phase at the solid-solid-liquid phase tri-junction (θ).

$$a_{(\alpha,\beta)} = \left(\frac{T_E}{L}\right)_{(\alpha,\beta)} \sigma_{(\alpha,\beta)} \sin\theta_{(\alpha,\beta)} \tag{2.7}$$

Lastly, Q^R is a constant which depends on the diffusion coefficient, D, and the compositional difference between the alpha and beta phases, denoted by C_o. This relation is shown in figure 2.1

$$Q^R = \frac{4(1+\zeta)}{D\zeta} C_o M \tag{2.8}$$

Here, M is a geometric parameter which is a summation of Bessel functions, $J(r)$, which are artifacts of the solution of the diffusion equation. The parameter, ζ_n are the n^{th} root of the Bessel function $J_1(r)$.

$$M = \sum_{n=1}^{\infty} \frac{1}{\gamma_n^3} \frac{J_1^2\left(\frac{r_\alpha \gamma_n}{r_\alpha + r_\beta}\right)}{J_0^2(\gamma_n)} \tag{2.9}$$

It should also be noted that the value of the characteristic rod spacing, R, is not the distance between the rods; rather, it is based on the volumetric extent of the major phase between rods.

$$R = r\sqrt{1+\zeta} \tag{2.10}$$

In this relation r is the radius of the rods. R is approximately one half of the average real rod spacing.

The Jackson-Hunt model further examines the interface shape of the two solid-liquid interfaces using the local composition field and the surface energy. The calculation of the interface shape showed that regular eutectic system develops with an isothermal interface. It is this isothermal approximation which is primarily questioned in the development of irregular eutectic models [74]. However, the thermal gradients required to influence the deviations observed in irregular systems are extreme.

2.2.2 Micro-Gravity Ambiguities

One of the motivating issues of eutectic systems is the ambiguity between ground and space based eutectic formation [85, 84]. This is of a particular interest in this study since funding for this project was provided by NASA. These studies conducted on Skylab were originally implemented to explore the utility of low gravity environment on directional solidification. There have also been a variety of ground based studies examining the impact of various perturbations to the eutectic system. These include examinations of the effects of forced convection [88], thermal convection [30], vibration [18], and buoyancy effects

in the liquid [23]. While it is apparent that convection can have a dramatic impact on the directional solidification of both laminar [2, 90] and rod [19] eutectic systems, the details of the interface kinetics of irregular eutectic systems needs to be examined by simplifying the problem first, then adding in other asymmetries. This work was conducted to provide a simple model capable of properly evaluating the interface kinetics while also providing a method to explore the potential impact of convection.

2.2.3 Past Simulations

The use of computational modeling on eutectic systems is not a novel approach to examining eutectic systems. The first computational modeling of the regular eutectic interface were conducted was conducted using resistive paper to Laplace's equations along the interface [56]. This was done to solve the diffusion field in front of the interface. Computational modeling has also been conducted using more conventional means. Karma examined growth of laminar eutectics using a phase field model. Solutions to the phase field equations were calculated on a two dimensional lattice and reproduced the undulations seen in eutectic systems are off eutectic composition or are conducted using too large of an inter-laminar spacing [63, 64]. More phase field modeling was conducted by Drolet in 2000 [31]. Later, Popov and Wilcox also used a one dimensional phase field model [86]. Similar phase field models were also employed to examine the stability of tri-phase junction [1] of laminar systems. Other continuum models have also been applied to the laminar eutectic system such as finite volume [106].

MC simulations using Metropolis method were also conducted [104, 73]. However, while MC simulations using the Metropolis algorithm describe the equilibrium state of interfaces they do not track the kinetics of a system since the relaxation path to equilibrium is non-physical.

2.3 Rod Eutectic Simulations

As previously stated, the JGT lattice gas model shares the same Hamiltonian as an ideal solution liquid in contact with a regular solution solid. With this model it is possible to construct an eutectic system where the A and B atoms self assemble into two separate phases. The challenge is thus, to develop systems using the input parameters discussed in chapter 1 to produce the growth of stable rods.

This task is accomplished by constructing a system with an equilibrium phase diagram of a binary eutectic then using the Jackson-Hunt model to estimate appropriate simulation cell geometry and diffusion characteristics. The relative importance of each of these steps is shown in figure 2.2.

2.3.1 Equilibrium Phase Diagrams

The compositional equilibrium phase diagram displays the composition of the liquid and the solid which produces no net movement of the interface as a function of temperature. For the case of a binary liquid in contact with a binary solid this occurs when the chemical potentials of both systems are equal. Expressions for chemical potentials are achieved by examining the Gibbs free energies of both the liquid (F^L) and solid (F^S) phases.

$$F^L = k_B T \left[N_A^L \, ln \left(\frac{N_A^L}{N_A^L + N_B^L} \right) + N_B^L \, ln \left(\frac{N_B^L}{N_A^L + N_B^L} \right) \right] \tag{2.11}$$

$$\begin{aligned} F^S &= -\frac{Z}{2} \left[N_A^S \, \Phi_{AA} + N_B^S \, \Phi^{BB} \right] - T \left[\Delta S_A \, N_A^S + \Delta S_B \, N_B^S \right] && (2.12) \\ &+ Z \, W \, \frac{N_A^S \, N_B^S}{N_A^S + N_B^S} && (2.13) \\ &+ k_B T \left[N_A^S \, ln \left(\frac{N_A^S}{N_A^S + N_B^S} \right) + N_B^S \, ln \left(\frac{N_B^S}{N_A^S + N_B^S} \right) \right] && (2.14) \end{aligned}$$

In these expressions N_A^S, N_A^L, N_B^S, N_B^L are the number of solid and liquid A and B atoms in the solid and liquid systems respectively. While W is defined as:

$$W = \frac{1}{2} \left(\Phi_{AA} + \Phi_{BB} \right) - \Phi_{AB} \tag{2.15}$$

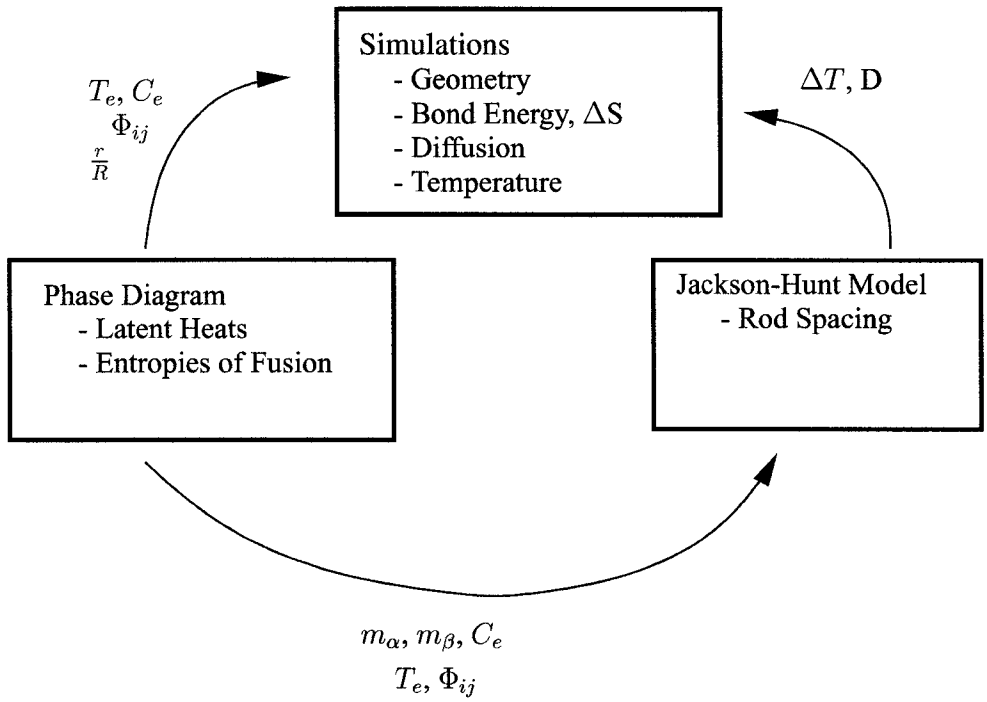

FIGURE 2.2. Flow Eutectic Simulations

While the kMC simulations do not require the calculation of an equilibrium phase diagram or the use of the J-H model, the two are used to acquire starting conditions for this eutectic study. The above shows the relationship between the input parameters of the kMC simulations and the calculated phase diagram and the J-H model.

The parameter W is significant in determining the composition of the α and β phases since it is a measure of strength of the A-B atom interaction. When W is greater than one, the solution tends to phase separate into separate phases, while when W is less than one the solution tends to order into a system of alternating A and B atoms. When W is equal to one the solution is ideal.

At equilibrium the chemical potentials (μ) in the solid and liquid phases of both the A and B species are equal.

$$\mu^L_{A,B} = \frac{\partial F^L}{\partial N^L_A} = \mu^S_{A,B} = \frac{\partial F^S}{\partial N^S_A} \tag{2.16}$$

Leading to the pair of equations 2.17 and 2.18.

$$\ln \frac{X^L_A}{X^S_A} = \frac{Z}{2k_BT}\Phi_{AA} + \frac{\Delta S_A}{k_B} + \left(1 - X^S_A\right)^2 \frac{ZW}{k_BT} \tag{2.17}$$

$$\ln \frac{X^L_B}{X^S_B} = \frac{Z}{2k_BT}\Phi_{BB} + \frac{\Delta S_B}{k_B} + \left(1 - X^S_B\right)^2 \frac{ZW}{k_BT} \tag{2.18}$$

where X is the number concentration of the individual species in each phase.

$$X^S_A = \frac{N^S_A}{N^S_A + N^S_B} \tag{2.19}$$

Thus the concentrations of A and B atoms in the solid and liquid phases also sum up to one.

$$X_A + X_B = 1 \tag{2.20}$$

These systems of equations were solved numerically to acquire the temperature dependence of the composition of both the α and β phases. This was done by using Brent's method [87] for finding the roots in *Numerical Methods in C*:

$$F_{solve}\left(X^S_A, T\right) = 1 - X^S_A \, exp\left(\frac{Z}{2k_BT}\Phi_{AA} + \frac{\Delta S_A}{k_B} + \left(1 - X^S_A\right)^2 \frac{ZW}{k_BT}\right) \tag{2.21}$$

$$\left(1 - X^S_A\right) \, exp\left(\frac{Z}{2k_BT}\Phi_{BB} + \frac{\Delta S_B}{k_B} + \left(X^S_A\right)^2 \frac{ZW}{k_BT}\right) \tag{2.22}$$

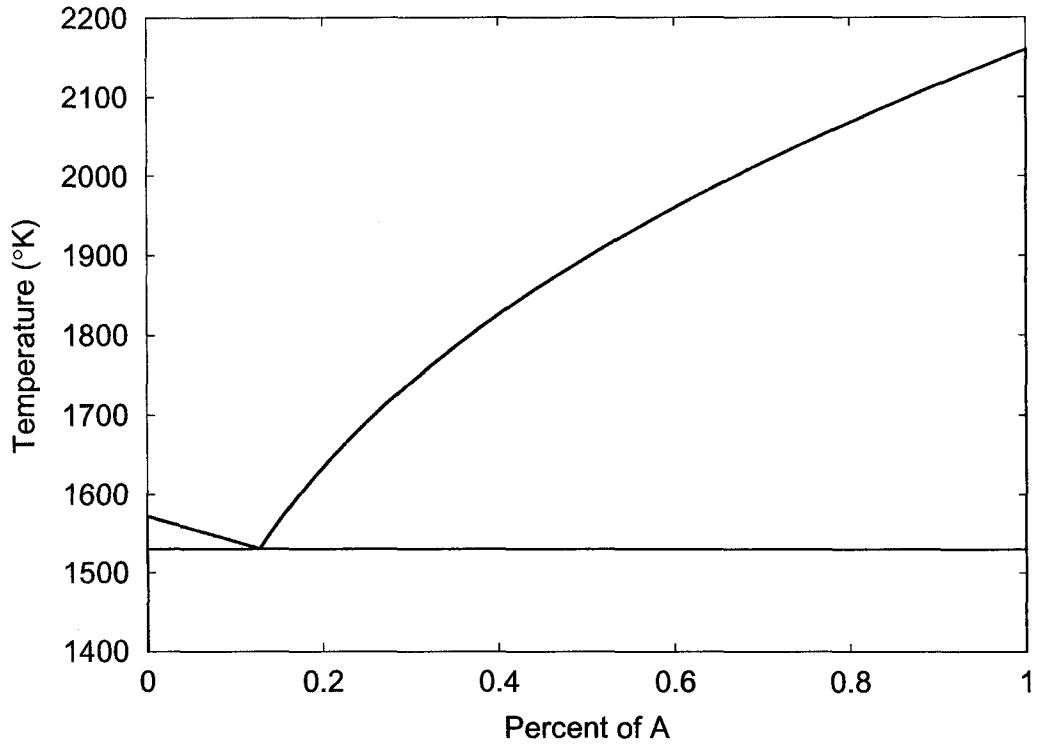

FIGURE 2.3. Sample Phase Diagram

In the binary eutectic systems studied, the α and β phases contained very little of the second component. The solidus lines in the phase diagram above are indistinguishable from the axis. This phase diagram was derived from the following bond energies: $\Phi_{AA}/k_B = 2820°K, \Delta S_A = 2.5k_B, \Phi_{BB}/k_B = 3000°K, \Delta S_B = 5.0k_B, \Phi_{AB}/k_B = 500°K$

This method was employed to isolate the physical roots since between the melting temperatures of the pure A and B systems there exist three roots to equation 2.22, one of which is non-physical. Figure 2.3 displays the results of one of these calculations.

There are two major attributes of phase diagrams sought after for this study. First, systems were chosen for the α and β phases which were composed of mostly pure A or B atoms. This occurs when the solidus lines are very close to the y-axis. Second, systems were chosen for eutectic compositions of 10% number fraction minor phase. This was to assure that the system will grow as rods.

2.3.2 Simulation Cell Construction

Simulations of a rod eutectic system are started with a simulation cell consisting of a liquid of randomly distributed A and B atoms and a solid of columns of pure A embedded in an B matrix. The rods were arranged in a close packed formation in the simulation cell using periodic boundary conditions normal to the growth direction. This arrangement is displayed in figure 2.4. While this lattice gas model is fully capable of spontaneously developing a micro-structure, simulations were initiated with these two phases. The process of nucleating rods has been observed in simulations where the chosen rod spacing was too large for stable rod growth and new rods formed on the major phase. The rod positions and radii were not confined in the simulation cell, however the simulation cell does place an upper limit on the rod spacing. Thus, the size of the simulation cell is an important parameter in these simulations.

The simulation cells themselves also have a finite size in the growth direction. For the sake of simplicity, simulations were conducted on completely closed system with a fixed size. The number of A and B atoms in these simulations were conserved.

2.3.3 Use of Jackson-Hunt model

While the rod eutectic simulations does not require the implementation of the Jackson-Hunt model, the model was used as a guide to acquire a starting point for stable rod growth. Comparison to the Jackson-Hunt model also provide a sanity check for the use of the JGT model. After an appropriate equilibrium phase diagram was selected, the remaining parameters; simulation cell size, simulation under-cooling and diffusion coefficient needed to be selected. The first of these, simulation dimensions, is easy since the simulation dimension is limited to the amount of computational power available. For these systems we focused on simulations with rods $\sim$10 lattice units in radii to keep the simulation size manageable. With this restraint it is possible to compute an appropriate under-cooling using

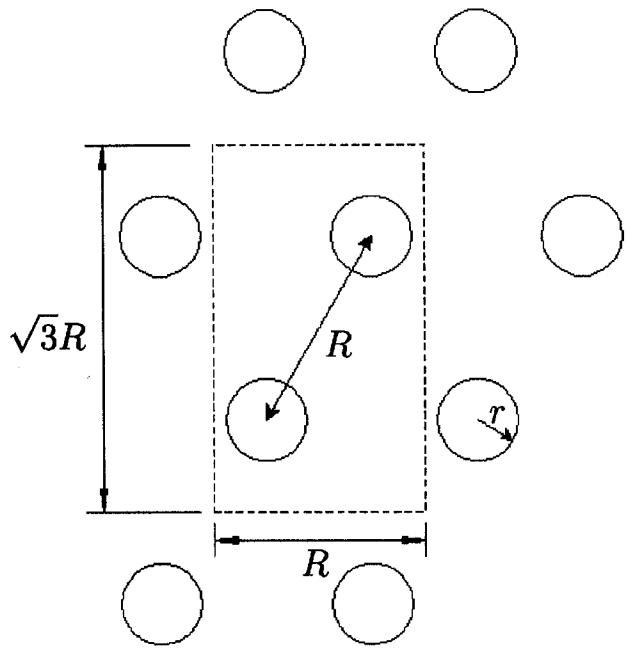

FIGURE 2.4. Simulation Cell Geometry

Rods of solid A atoms are arranged in the simulation cell with semi-periodic boundary conditions in a closed packed formation. This is done with a simulation cell of $\sqrt{3}\ R$ by R where R is the rod spacing. Note that this is not the same R as used in the text rather it is R_{sim} as used in table 2.1. The rod radius r is dependent on the eutectic composition.

equation 2.1.

$$\Delta T \cdot R = C_1 \left(\Phi_{ij},\, T_E, C_E,\, m_\alpha, m_\beta,\, \sigma_{\alpha,L},\, \sigma_\beta,\, L,\, sin\left(\theta_{\alpha,\beta}\right)\right) \tag{2.23}$$

There two distinct problems with evaluating the constant C_1 used in the lattice gas model: acquiring the values of the inter-facial free energies (σ) and retrieving the angles at the tri-phase junction ($\theta_{\alpha,\beta}$). Both of these problems are linked, and the solutions are found using estimates of the interfacal free energies of the system. For our purposes these estimates of these values were based on free bond counting to calculate the surface free energy. While this method for calculating the surface tensions of the interfaces is not exact, it does provide a good estimate. For regular eutectic systems the two individual phases will have interfaces with isotropic surface free energies, the surface free energy is independent of orientation. This interfacal energy can be estimated as one half the product of the cube-root of the atomic volume (a) and the latent heat of the system.

$$\sigma_{\alpha,L} = \frac{L \cdot a}{2} = \frac{Z\,\Phi_{AA}\,a}{4} \tag{2.24}$$

The difficulty with acquiring the angles of the individual phases is linked to the calculation of the surface free energies. These angles are displayed in figure 2.5. While this is not explicitly stated in Jackson-Hunt, there is a force balance of surface tensions at this tri-junction. Thus, the angle of the interface is a function of the surface tensions of the interface.

$$\sin\theta_\alpha = \frac{\sigma_{\alpha L}^2 + \sigma_{\alpha\beta}^2 - \sigma_{\beta L}^2}{2\sigma_{\alpha L}\sigma_{\alpha\beta}} \tag{2.25}$$

The surface tension of the three interfaces may be written in terms of the solid-solid bond energies:

$$\sin\theta_\alpha = \frac{\Phi_{AA}^2 + 4\,W^2 - \Phi_{BB}^2}{4\,\Phi_{AA}\,W} \tag{2.26}$$

The second parameter with which the J-H model aids to approximate is the diffusion coefficient. In particular the input parameter θ, which is is the ratio of the rate of solute

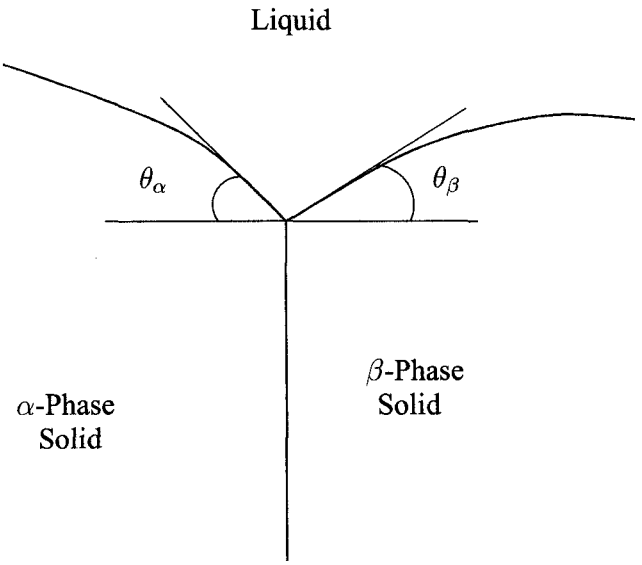

FIGURE 2.5. Angles of the Solid Phases

There exists a force balance of surface tensions at the junction between the solid alpha, solid beta and liquid phases. It is this force balance which dictates the angles of the the solid-liquid interfaces of both the alpha and beta phases. Both θ_α and θ_β are defined in the above figure.

diffusion in the liquid to the rate at which atoms join the crystal at a repeatable step site. This is accomplished by examining equations 2.2 and 2.8 and using the expected interface growth rate. In general the velocity of the interface may be written as in equation 2.27.

$$V = \left(\frac{\nu_k^+ - \nu_k^-}{\nu_k^+} \right) \nu_k^+ \rho \Omega \tag{2.27}$$

Here ν_k^+ and ν_k^- are the rate with which atoms arrive and depart repeatable step cites, ρ is the density of repeatable step sites, and Ω is the distance the interface advances with the arrival of an add-atom. The arrive and departure rates are provide by the JGT model with equation 1.19 and 1.20 for a repeatable step site. For the add-atom departure rate this is when half of the solid atom's nearest neighbors are liquid. For simplification the focus is on the growth of the major phase. However, both phases must grow at the same rate. A expression for θ may then be written using the input parameters of the system using equations 2.2, 2.8, 1.21, and 2.27.

$$\theta = 24 \left(\frac{R}{a} \right)^2 C_o M \left(\frac{\nu_k^+ - \nu_k^-}{\nu_k^+} \right) \frac{(1+\zeta)\, a}{\zeta\, a^R} \tag{2.28}$$

An example of the intermediate values of these calculations can be found in table 2.1 for one of the stable eutectic systems. These values were retrieved using a spread sheet calculation.

2.4 Results

Simulations of stable growing rod eutectics were first conducted using a simple cubic lattice oriented in the $\{100\}$ growth direction. Initially simulations were conducted at the eutectic composition. However, these simulations failed when the major phase enveloped the minor phase. Guided by laboratory studies, the minor component's composition in the liquid was increased by 30% and rod growth occurred.

Initially rods were observed to modulate in thickness with the initial rod spacing. Similar behavior has been observed in laminar systems both in laboratory and simulations

studies when inter-laminar spacing was too large [62] or when the liquid composition was off eutectic composition [105]. This modulation, followed by the rod structure breaking up and reforming a new structure, was eliminated by shrinking the size of the simulation cell. An example of a stable rod system is displayed in figure 2.6. The input parameters, including the J-H model properties of this system are shown in table 2.1. While the results were guided by the J-H model, the original calculations of this model had errors. There were difficulties in determining the relationship between R in the J-H model (R_{J-H} in table 2.1), r and the dimensions of the simulation cell. These errors were discovered after the simulation was conducted, however this finding does not invalidate the results.

From this result, and others not shown in this document, we have seen that there is good agreement with the J-H model regular eutectic systems. Of particular importance is the product $\Delta T \cdot R$. For a set ΔT the choice of simulation size is very important, and systems conducted to far away from the calculated simulation cell dimensions fail. However, we have also seen that the choice of θ is not as critical and mostly effects the width of the diffusion field in front of the interface.

The largest obstacle in these studies was the about of time required to run simulation. A full simulation could run for months before there was full confidence in the results. Much of this computation time was used by diffusion events in the liquid. Also, since all initial interfaces were flat and a combination of growth and melt back processes along the interface were observed to generate the steady state interface shape and growth behavior. Thus simulation cells were chosen to be large enough in the growth direction to show the micro-structure development and the initial solid was made thick enough so that melt-back would not reach the bottom of the simulation cell. There are many possible improvement that could have been made to these simulations to improve their speed however delay on implementing this improvements outweighed getting initial results.

Input Parameters		Intermediates		Final Parameters	
Φ_{AA}	2820 $k_B \cdot {}^\circ K$	a_α	719.2 a	$2\,m\,a^R$	1797 ${}^\circ K \cdot a$
Φ_{BB}	3000 $k_B \cdot {}^\circ K$	a_β	739.9 a		
Φ_{AB}	500 $k_B \cdot {}^\circ K$	a^R	2.577 a		
ΔS_A	2.5 k_B				
ΔS_B	5.0 k_B				
m_α	3710 ${}^\circ K$	m	348.8 ${}^\circ K$		
m_β	385	θ_α	55°		
T_e	1762.6 ${}^\circ K$	θ_β	57°		
Z	6				
ζ	9	M	0.0395		
ρ(assume)	1				
				$\theta_{proposed}$	51.2
ΔT	68 °K	r	8.3 lattice units	θ_{used}	24.58
R_{cell}	50 lattice units	R_{J-H}	26.25 a	$\Delta T \cdot R_{J-H}$	1785 ${}^\circ K \cdot a$
C_{liq}	13% A atoms				

$a = 1$ lattice units, for a SC lattice.
(note: $a = \sqrt[3]{atomic\,volume}$)

TABLE 2.1. Stable Regular Rod Eutectic System
In this table R_{cell} is the size of the simulation cell as defined in figure 2.4 and R_{J-H} is the R parameter found in the J-H model.

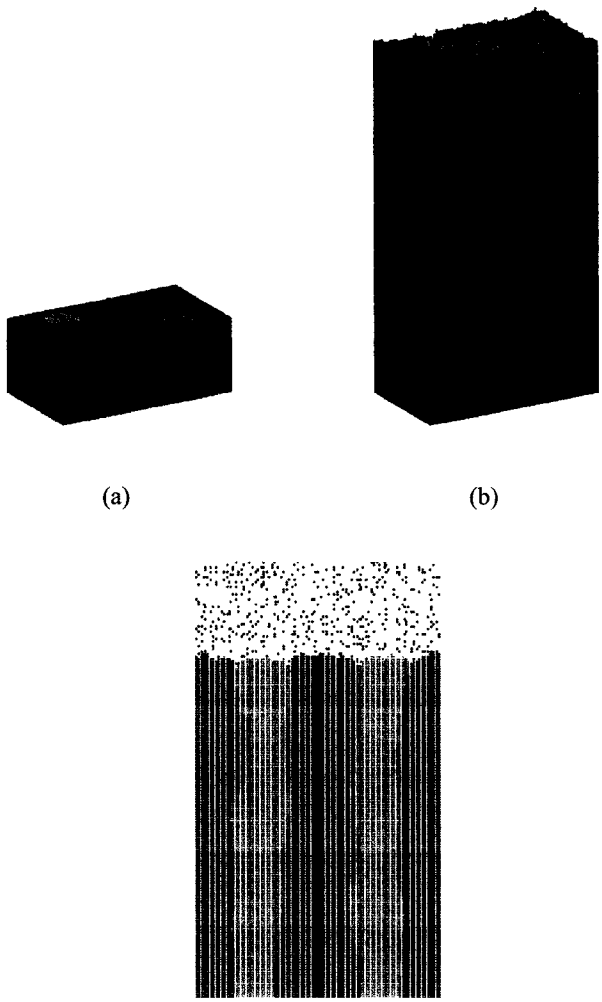

(a) (b)

(c)

FIGURE 2.6. A Typical Simulation

Results (a) and (b) are 3D perspective views of the solid atoms in the simulation cell. (c) is a diagonal slice through the simulation cell of figure (b) where A and B solid atoms and B liquid atoms are displayed. The simulations cell has dimensions of 50 by 87 by 230 unit-cells and the initial has a radius of 8 unit-cells. Simulation's input parameters shown in table 2.1. Figures were rendered using Raster3D [77].

2.4.1 Irregular Eutectics

Irregular eutectics have previously been modeled using adaptations of the Jackson-Hunt model [35, 75, 100]. However, these analytical models do not address the nucleation of new atomic layers on the faceted phases. Rather, they focus on application of thermal gradient applied to the Jackson-Hunt model. The original motivation behind these approaches was to examine the Si-Al system where Si phase separates into rods in the Al major phase. In these systems rods of silicon are faceted phase and the aluminum surface is smooth.

During the examination of systems thought to be regular eutectics using a simple cubic lattice oriented in the $\{111\}$ direction irregular eutectic behavior was observed. It was at this time that interest in examining the roughening behavior of the binary alloy was initiated. With a simple cubic simulation cell oriented in the $\{111\}$ direction and both A and B atoms having the same ΔS's, the surface roughness of the two phases was visually different. These results are shown in figure 2.7. Here the minor phase clearly shows faceting while the interface of the major phase is rougher. The Jackson-Hunt calculated rod spacing, shown in table 2.2 is also roughly twice as large the one used in the simulation. Systems like this one were examined with the major facets in the plane of the interface and all of failed to the minor phase growing too slowly.

At this point, the project changed focus from SC to FCC lattices since the SC $\{111\}$ simulations cell does not tessellate in the same way as the SC $\{100\}$ simulation cell does. This is due to the methods used to construct the simulation cell. This error is apparent after examination of 3D perspective view of figure 2.7. In this figure, the facets form an isosceles triangle rather than an equilateral triangle, as expected. This image has been distorted to force the simulation cell to look like a regular rectangular prism, while, in reality it is an trapezoidal prism. An FCC lattice was chosen since the $\{111\}$ can facet before the $\{100\}$ planes since the $\{111\}$ has more in the plan nearest neighbors than the $\{100\}$ plane, thus effecting the value of the Jackson α-factor.

These results generate two major questions. One, what is the surface roughening be-

Input Parameters		Intermediates		Final Parameters	
Φ_{AA}	2500 $k_B \cdot {}^\circ K$	a_α	408.0 a	$2\,m\,a^R$	1125 $^\circ K \cdot a$
Φ_{BB}	1750 $k_B \cdot {}^\circ K$	a_β	254.3 a		
Φ_{AB}	700 $k_B \cdot {}^\circ K$	a^R	2.6781 a		
ΔS_A	5.0 k_B				
ΔS_B	5.0 k_B				
m_α	1314.5 $^\circ K$	m	210.05 $^\circ K$		
m_β	250	θ_α	52.53°		
T_e	1028.2 $^\circ K$	θ_β	29.65°		
Z	6				
ζ	9	M	0.0395		
ρ(assume)	1				
				$\theta_{proposed}$	23.9
ΔT	9.2 °K	r	11.7 lattice units	θ_{used}	2.6
R_{cell}	71 lattice units	R_{J-H}	37.1 a	$\Delta T \cdot R_{J-H}$	341.50 $^\circ K \cdot a$
C_{liq}	13% A atoms				

$a = 1$ lattice units, for a SC lattice.
(note: $a = \sqrt[3]{atomic\,volume}$)

TABLE 2.2. Stable Irregular Rod Eutectic System
Simulation conducted on with a simple cubic interface oriented in the <111> direction. In this table R_{cell} is and approximation of the size of the simulation cell as defined in figure 2.7.

havior of a binary alloy system? Two, where is the surface roughening transition for the JGT lattice gas system? These two question are answered in the next two chapters.

2.5 Conclusion

I developed and demonstrated the use of a JGT model system capable of simulating the growth of stable rod eutectics. The simulations have successfully used the Jackson-Hunt model as a guide to provide appropriate starting conditions. These simulations exhibit behaviors similar to experimentally observed eutectic structures.

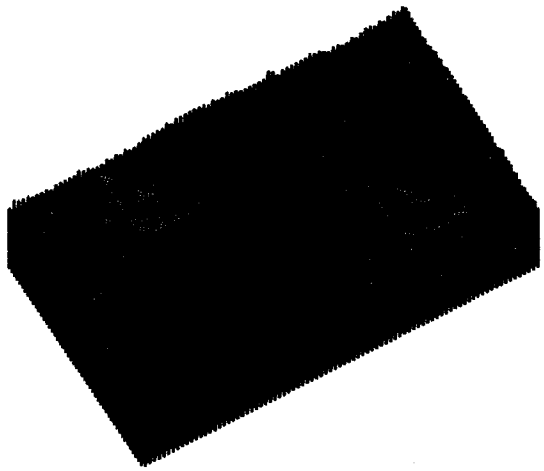

(a)

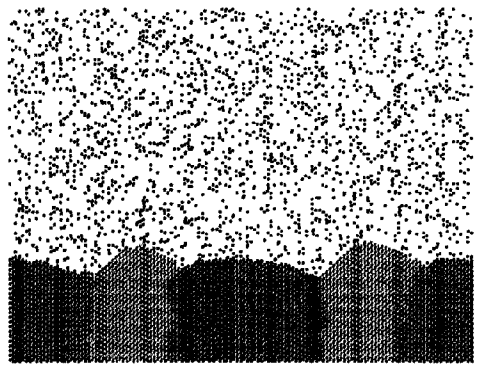

(b)

FIGURE 2.7. Irregular Rod Eutectic

Simulation conducted on a simple cubic lattice oriented in the $\{111\}$ growth direction. Both A and B atoms gave the same ΔS. However, the surface roughness characteristics of both the alpha and beta phase are clearly different. Facets form on the $\{100\}$ faces. The 3D perspective view of figure (a) is distorted into a rectangular simulation cell. Figure (b) is a diagonal slice though the simulation cell. $\Phi_{AA}/k_B = 2000°K, \Delta S_A = 5.0k_B, \Phi_{BB}/k_B = 1650°K, \Delta S_B = 5.0k_B, \Phi_{AB}/k_B = 300°K T_E = 1028.2°K, \Delta T = 9.2°K$. Figures were rendered using Raster3D [77].

CHAPTER 3

THE SURFACE ROUGHING TRANSITION

3.1 Surface Roughness

One of the most influential characteristics in crystal growth is surface roughness. This is apparent since as the surface becomes rougher the repeatable step site density increases. Thus, surface roughness plays a crucial role in rate of solidification as a function of under-cooling. The interface kinetics are dramatically different on either side of the surface roughening transition. Below the transition, the growth rate of the solid is limited by the production of repeatable step sites. While above the transition there is no activation energy barrier to produce a repeatable step cite and the growth rate linear with under-cooling. In the case of a defect free, smooth surface repeatable site formation is controlled by the rate which critical nuclei are formed. The surface roughening transition occurs when the activation energy to form a critical nucleus goes to zero.

The first models concerning the growth rate of a smooth solid surface was conducted by Burton, Cabrera, and Frank [15]. In this paper Frank developed an analytical model of the step motion as a function of supersaturation based on the kink site density of the step edge. This model was used to propose a process in which a flat interface could circumvent the slower growth rates of surface nucleation using the geometry of screw dislocations. In the second part of the paper, Burton and Cabrera highlighted the importance of the spiral step growth model to smooth interfaces by solving the two level problem using Onsager's method [82] and presenting the extension to multiple level solutions. Their conclusion of examining this problem was, "...the existence of a transition temperature will not have any influence on the kinetics of growth of the crystal surface" [15]

In 1958 Jackson introduced the α-factor as a predictive measure of surface rough-

ness [51, 53].

$$\alpha = \frac{L}{k_B T_M} \frac{\eta}{Z} \tag{3.1}$$

This factor is comprised of the latent heat L, melting point T_M, configuration number of the lattice Z, and the number of nearest neighbors in the plane of the surface η. The Jackson α-factor is a unit-less parameter which is measure of the surface tension of the interface. Experimental solid-liquid interfaces below a critical value of $\alpha = 2$ were rough while above this value the interfaces were smooth at the atomic level.

Later in 1971, Leamy and Jackson [71] compared Monte Carlo (MC) simulations of a solid-on solid SOS model to zeroth order, Bragg-Williams, and first order, Bethe approximations, continuum expansions of SOS model. The roughening behavior of both of these models and the MD simulations have similar results and reproducing experimentally observed systems. The roughening behavior of the exact two level system, however, deviated theses observation of interface roughness as a function of α-factor. The agreement of these three model ends however with the treatment the kinetic nature of the interface. Both of the continuum models do not treat the formation of critical nuclei [69].

3.1.1 Height-Height Correlations

While the surface roughening transition has a dramatic influence on the kinetics of the system, it is only seen as a weak discontinuity in the equilibrium system. This difficulty in determining the transition using computer modeling is compounded with the problem of in defining and measuring a surface roughness. Previously the most utilized method to evaluating the surface roughening transition has been though the calculation height-height correlations of the interface. This method has been used both in the laboratory and experimentally. The height-height correlation function is a measure of how perturbations in the growth direction become uncorrelated along the plane of the interface. This function is showed in equation 3.2.

$$G(r) = \left\langle (h_o - h_i)^2 \right\rangle \tag{3.2}$$

where G(r) is the variance of the difference of heights of columns of solid separated by a distance r. Above the transition, the solid surface can support a wide variety of undulations. In contrast, the smooth surface remains flat and only supports very long wavelength perturbation and the height-height correlation function is less dependent of r.

Chui and Weeks showed with a solid on solid (SOS) Hamiltonian that the height-height correlation function, G(r), of the rough interface has a logarithmic behavior [22].

$$G(r) = \frac{K_\infty}{\pi}\left(ln(r) + c\right) \tag{3.3}$$

where K_∞ is a renormalization coupling constant and c is a non-universal constant. This analysis was conducted using Kostelitz's [65] approach which is used to examine correlation lengths in 2D systems. With this analysis it was shown that there is a weak singularity denoting the surface roughening transition at a critical value of $K_\infty = \frac{2}{\pi}$

The convention of defining an interface above or below the surface roughening transition has its origins in viewing the transition existing about a critical temperature. This is a point of confusion when viewing the transition with the Jackson α-factor. This is because the characteristic temperatures used the original studies conducted by Chui and Weeks have a reciprocal relationship with the α-factor. Thus, interfaces below the surface roughening transition referees to systems which have an αs above α_c and above the transition referees to αs below α_c.

The surface roughening transition has been extensively studies using lattice gas models. Shugard, Weeks and, and Gilmer [92] examined the transition with MC simulations on the same SOS model as examined by Chui and Weeks. This study measured the critical α-factor on their simple cubic lattice to exist between 3.2 and 3.4. Other surface roughness studies have been conducted on diamond cubic lattice and evaluated using height-height correlations. These studies by Woodraska [102] on the $\{111\}$ diamond cubic interface and observed a different critical value for the surface roughening transition and attributed this discrepancy to pre-roughening behavior [102] The difficulty with this conclusion is that the SOS model for the diamond cubic lattice has complicated inter-level interaction such that

there is a complicated level-level interaction.

This chapter presents a method of calculating the kinetic coefficient of a solid-liquid interface using time correlations. This method was also used to determine the surface roughening transition of this lattice gas model since there is a distinct and abrupt change in the kinetic behavior of the system at this point.

3.2 Fluctuation Dissipation Theory

Fluctuation dissipation theory is based on Onsager's regression hypothesis which was first used in 1931 [81]. The hypothesis states that a system relaxes from spontaneous microscopic fluctuations in the same way that it relaxes from a macroscopic non-equilibrium perturbations.

While this statement was first stated by Onsager, it was proved by Callen and Welton in analyzing Johnson noise [17]. This powerful assertion states that by the examining rates of which thermal fluctuations about an equilibrium position loose their instantaneous effect on the loose on the system, it is possible to extract the macroscopic time constants of the same global system when it is slightly perturbed from it equilibrium position. Thus, the characteristic time extracted from examining the time correlation function of a dynamic variable who's average value is not time dependent is the same characteristic time of a this system with small macroscopic deviations from equilibrium. This is provided that the restoring force in both perturbations are the same. Examples of a variety of applications have been shown by Chandler [20].

The time correlation function is an autocorrelation function used to determine how fast a dynamic parameter ($D(t)$) looses its memory of a past configurations. For example, if a system is displaced from its equilibrium state the time correlation function shows how quickly the system returns to its equilibrium state. This is assuming that there is a restoring force on that system which maintains the equilibrium position. The time correlation function of a dynamical parameter ($C_D(t)$) is thus a measure of the speed in which perturbations

of the system take to become uncorrelated. So that at $t = 0$, $C_D(0) = 1$ and at long times where there is no correlation between events as $C_D(t) \rightarrow 0$.

$$C_D(t) = \frac{\langle (D(t) - \bar{D}) \cdot (D(0) - \bar{D}) \rangle}{\langle D^2(0) \rangle} \tag{3.4}$$

where $\bar{D}$ is the average value of D.

Assuming that perturbations decay by a single pathway, or because of a single mechanism, and this mechanism is independent of the past history of system (Markovian style events) the time correlation function will take on the form of

$$C_D(t) = exp\left(-\frac{t}{\tau}\right) \tag{3.5}$$

where τ is the characteristic time of that pathway.

If there are more than one of these pathways then each pathway will impact the time correlation function depending on the strength of the pathway(C_n). Each of these will intern effect the time correlations function as in equation 3.6.

$$C_D(t) = C_1\, exp\left(-\frac{t}{\tau_1}\right) + C_2\, exp\left(-\frac{t}{\tau_2}\right) + ... + C_m\, exp\left(-\frac{t}{\tau_m}\right) \tag{3.6}$$

Here the sum of the strength of the pathways must equal one.

Fluctuation dissipation theory has been previous used to examine the kinetic behavior of the solid-liquid interface by observing the equilibrium behavior of the system. In 1997, Briels and Tepper [12] examined the fluctuation of the number of solid atoms in a MD simulation and related this behavior back to the kinetic coefficients of the system. In their study simulations conducted with constant pressure to maintain equilibrium. The kinetic coefficient is the constant relates the under-cooling of the interface to its growth rate.

In this study, the kinetic behavior of the solid-liquid interface was examined using fluctuations in the number of solid atoms as function of time in a kMC simulation cell needed to be examined. By defining the average number of solid atoms in the simulation as $\langle N_S \rangle$ over some time period, the dynamical parameter $N_S(t)$ was defined as

$$N_S(t) = N_S(t) - \langle N_S \rangle \tag{3.7}$$

Here $N_S(t)$ is the number of solid atoms at some time, t. The time correlation function then takes the form of

$$C(t) = \frac{\langle \Delta N_S(t) \cdot \Delta N_S(0) \rangle}{\langle \Delta N_S^2(0) \rangle} \tag{3.8}$$

In order to understand the nature of the time correlation function the macroscopic behavior of the interface must first be examined. The motion of the interface depends on the rate at which atoms arrive and depart the interface. Thus, the rate which interface moves, v may be written as

$$v = \frac{d\Delta z}{dt} = \frac{\Omega}{A}\frac{d\Delta N_s}{dt} \tag{3.9}$$

Here, Ω is the atomic volume and A is the atomic area in the plane of the interface.

For rough interfaces with small under-cooling, the growth rate of the solid is linear with under-cooling, as shown in chapter 1.

$$v = \beta \Delta T \tag{3.10}$$

Here β is the kinetic coefficient. At this point it is assumed that the interface is rough since the interface kinetics become very complicated for smooth interfaces. The method for calculating the kinetic coefficient is only applicable for rough interfaces. However, the time correlation function still examines the kinetic behavior of both the rough and smooth interfaces.

The next step is to develop a system containing a solid-liquid interface which when displaced from an equilibrium position system experiences a restoring to return to it equilibrium position. This is done in this system by applying a thermal gradient, $G = \frac{dT}{dz}$, on the system in the growth direction.

In a thermal gradient, if the interface grows by Δz, then the interface temperature is increased by $G\,\Delta T$ and the interface will melt. If it recedes by Δz is under-cooled and grows. When the interfaces moves by Δz the number of solid atoms of the system changes by $\frac{\Omega}{A}\,\Delta N_S$. We can then write the expression:

$$-\Delta T = \frac{\Omega}{A} G\,\Delta N_S \tag{3.11}$$

relating the under-cooling ΔT to the change in the number of solid atoms in the system. Here $\Delta T = T - T_M$, and it is negative since it represents an under-cooling of the system.

We can thus acquire a differential equation relating the time rate of change of the number of solid atoms in the system to the applied thermal gradient using equations 3.9, 3.10, and 3.11.

$$\frac{d\Delta N_S}{dt} = -\beta\, G\, \Delta N_S \tag{3.12}$$

The solution to this differential equation is

$$\Delta N_S(t) = \Delta N_S(0)\, e^{-\beta G t} \tag{3.13}$$

The time correlation function thus decays exponentially:

$$C(t) = e^{-\frac{t}{\tau}} \tag{3.14}$$

where the characteristic time τ is related to β and G by:

$$\tau = \frac{1}{\beta G} \tag{3.15}$$

3.3 KMC Study of interface

Following the construction of the system in the previous section, kMC simulations were conducted on a solid interface placed in a thermal gradient. The kMC events used in this study were the same as motivated in chapter 1 and implemented in chapter 2 with a slight change. Here the temperature each atom depends on it position in the simulation cell:

$$\nu_i^{LS} = \nu_o\, exp\left(-\frac{\Delta S_i}{k_B}\right) \tag{3.16}$$

$$\nu_i^{SL} = \nu_o\, exp\left(-\sum_j \frac{\Phi_{ij}}{k_B T(z)}\right) \tag{3.17}$$

Flat interfaces oriented perpendicularly to this thermal gradient were then constructed in a simulation with semi-periodic boundary conditions. To determine the surface roughening transition of the rod eutectic system discussed in chapter 2, these simulations were conducted on a FCC lattice oriented in the $\{100\}$ direction.

The melting point of the system was then set in the center of the cell so that the interface would not interact with the top and bottom boundaries of the cell, which were set to be solid or liquid respectively. Interfaces were then allowed to fluctuate about the melting point. Examples of these interfaces are displayed in figure 3.6. The number of solid atoms in the simulation cell was saved to a file at a rate 100 - 1000 faster than the measured time constant of the simulation while the total simulation was run 50 - 100 times this time constant. Table 3.1 shows a record of the FCC simulations conducted for this study. An example of the output of one of these simulations is displayed in figure 3.1. This graph displays the number of solid atoms at different times in the simulation and it is representative of the duration of simulations used in this study.

Since the surface roughening transition of FCC interfaces have not be previously been studied, the surface roughening transition of the simple cubic (SC) was examined. Results from both these studies are found in tables 3.1 and 3.2. Both the SC and FCC systems were studied using different sized simulation cells as and implemented with a few different magnitudes of thermal gradients.

3.3.1 Time Correlations

Time correlation functions were computed after the completion of the simulation. The exact nature the computation of the time correlation function is displayed in equation 3.18. The time correlation function was applied to several different time slices of the output file to acquire an understanding of the statistical nature of its computed values. These time

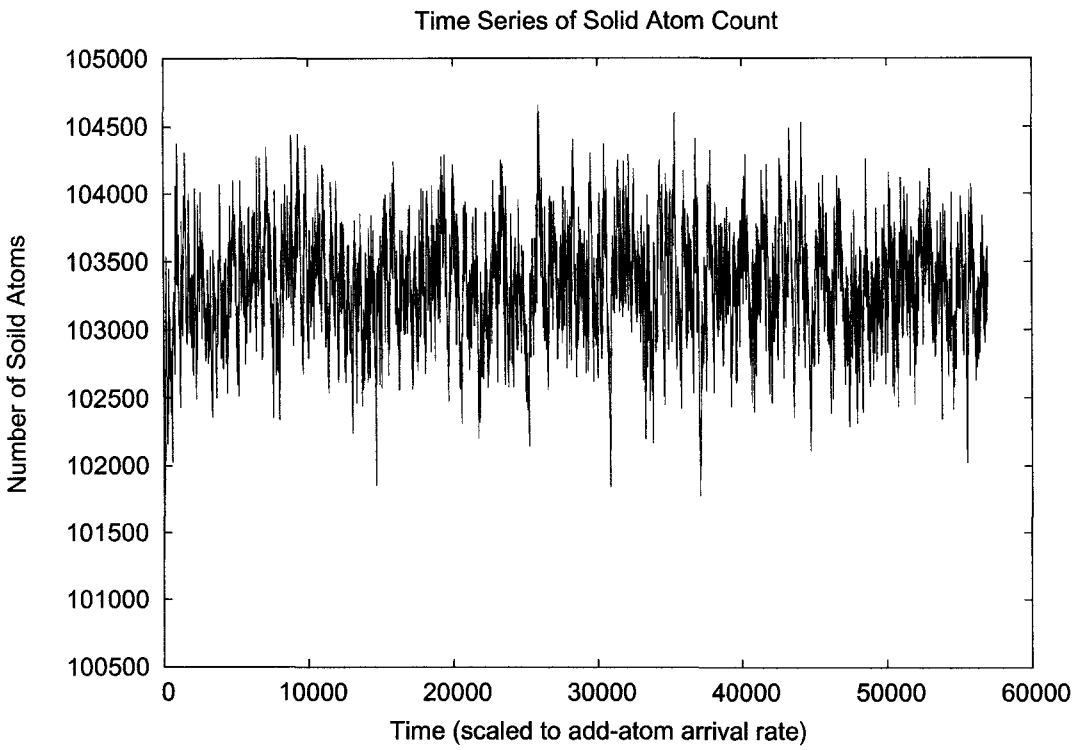

FIGURE 3.1. Time Series

The above plot displays the number of solid atoms in the simulation cell as a function of time. System fluctuates about the equilibrium position at the center of the simulation cell because of the imposed thermal gradient 1.0 °K per unit lattice $\sim$ (a). Simulation conducted with $\Delta S_A = 7.0\, k_B$ and $\Phi_{AA} = 116.7\,^{\circ}K\, k_B$ on a FCC lattice 50 by 50 unit lattices in size.

slices are expressed as time interval between $t = N$ and $t = M$.

$$\langle \Delta n(0) \cdot \Delta n(t) \rangle = \sum_{i,j=L,\, i<j}^{M} \frac{(\Delta n_i - \Delta n_j)\, \delta\left(t - (t_i - t_j)\right)}{N_{in\,bin}(t)} \tag{3.18}$$

In this summation n_i is the number of solid atoms in the simulation at time t_i. The function $\delta\left(t - (t_i - t_j)\right)$ in this equation is the Kronecker delta function of width Δt. This delta function is used to bin the difference of $\Delta n_i - \Delta n_j$ as a function of time. The number $N_{in\,bin}(t)$ is the number of difference in each of these bins. The bin's width is chosen to provide an adequate sampling for a time t. Correspondingly the denominator of the correlation function is computed by using equation 3.19.

$$\langle \Delta {N_S}^2(0) \rangle = \sum_{i=L}^{M} \frac{{\Delta n_i}^2}{N_{in\ bin}(t)} \tag{3.19}$$

A semi-log plot of a typical time correlation function is displayed in figure 3.2.

At this point, characteristic times may be extracted from the time correlation function. While the time correlation function may be fitted with equation 3.6, this study focused on the the most prevalent characteristic time of the the system and used a fitting function of

$$C(t) = C_o\, exp\left(-\frac{t}{\tau}\right) \tag{3.20}$$

using the nonlinear least-squares Marquart-Levenber method was used by the Gnu project's program 'fit.'

There were some difficulties in extracting the time constants just below the surface roughening transition. At this point it is possible to observe a few different time constants in a few of the time correlation functions. When this occurred, the time correlation function was fitted for the most dominating time constant. These extra time constants are not observable in all time correlations and may become less apparent even in comparing several time correlation functions from the same simulation.

The reciprocal of these characteristic times were then divided by the magnitude of the thermal gradient to attain a kinetic parameter. It is important to distinguish between the

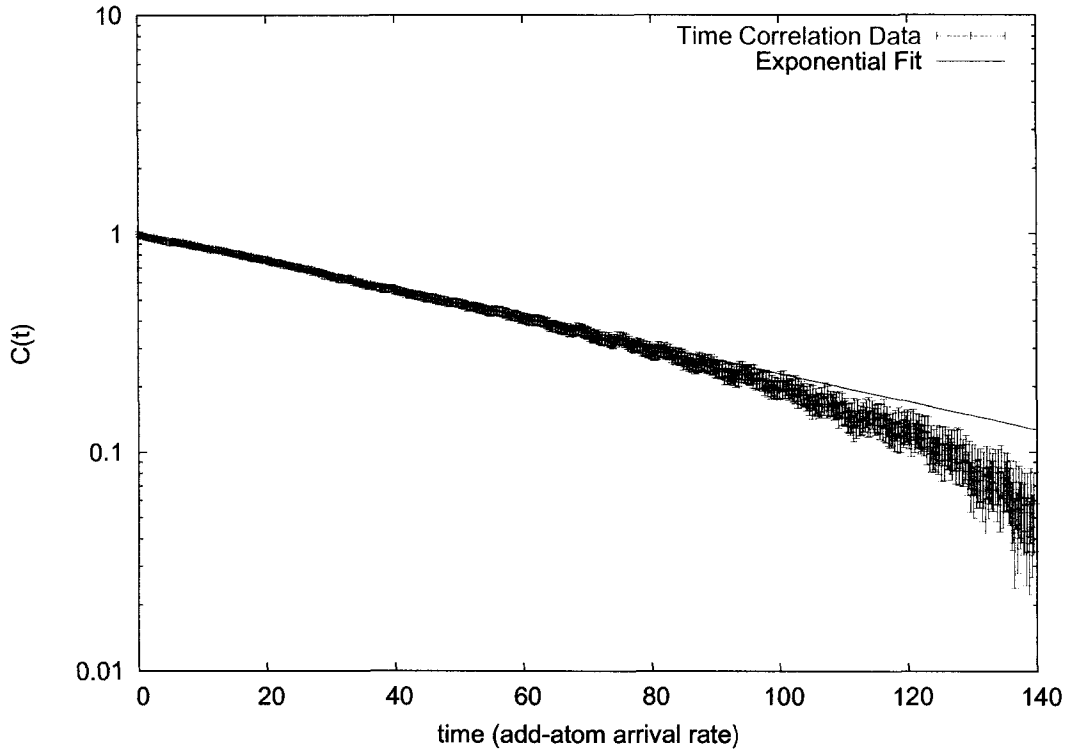

FIGURE 3.2. Time Correlation

This semi-log plot of time correlation is taken from data in figure 3.1 in the time interval of $3.19 - 3.65 \times 10^4 \nu_+$. The time correlation function shows an exponential decay from $t = 0$. The characteristic times of the system are measured by least squares to equation 3.14. In this example $1/\tau = 0.01483\ \nu_+$ when fit up $t = 50\, 1/\nu_+$. Error bars were calculated using equation 3.21.

measured kinetic parameter and the kinetic coefficient. This study examined the behavior of the interface above and below the surface roughening transition. Below the surface roughening transition the measured kinetic parameter is the kinetic coefficient of the system, while, above the transition, this is not the case. This distinction will be discussed in the next section.

In an attempt to understand the statistical nature of measurement the characteristic times, the statistics of acquiring the time correlation function were examined. Since the time correlation function is an average of values there is a discernible uncertainty in this measurement which depends on the number of points in each bin. This uncertainty is expressed in equation 3.21.

$$\delta C(t) = \frac{1}{\langle \Delta {N_S}^2(0) \rangle} \delta \langle \Delta n(0) \cdot \Delta n(t) \rangle + \frac{\langle \Delta n(0) \cdot \Delta n(t) \rangle}{\langle \Delta {N_S}^2(0) \rangle^2} \delta \left\langle \Delta {N_S}^2(0) \right\rangle^2 \quad (3.21)$$

The standard deviation of the means are expressed in equation 3.21 are just

$$\delta \langle \Delta n(0) \cdot \Delta n(t) \rangle = \frac{std\left(\langle \Delta n(0) \cdot \Delta n(t) \rangle\right)}{\sqrt{N_{in\,bin}(t) - 1}} \quad (3.22)$$

This error analysis is the bases for the one σ error bars shown in figure 3.2.

While this is the standard of the mean, evaluation the time correlation function of subsets of the total simulation suggested that this method of computing the error underestimates sampling nature of equation 3.18. In equation 3.18 the time correlation bins were using overlapping bins of time, thus there may be a problem with over sampling. Estimates the precession of the characteristic times sub-sets of the other systems were calculated by examining smaller non-overlapping sections of the compete simulation. Typically one simulation is broken up into 8 to 12 of these sections. It is the mean and the standard deviation of the mean of these values which have been displayed in figures 3.3 and 3.4 and reported in tables 3.1 and 3.2.

3.3.2 Surface Roughening Transition

The Ising lattice gas system has three distinct roughening regimes with respect to the α-factor. This behavior shown in figure 3.5. These three regimes separated by two phase

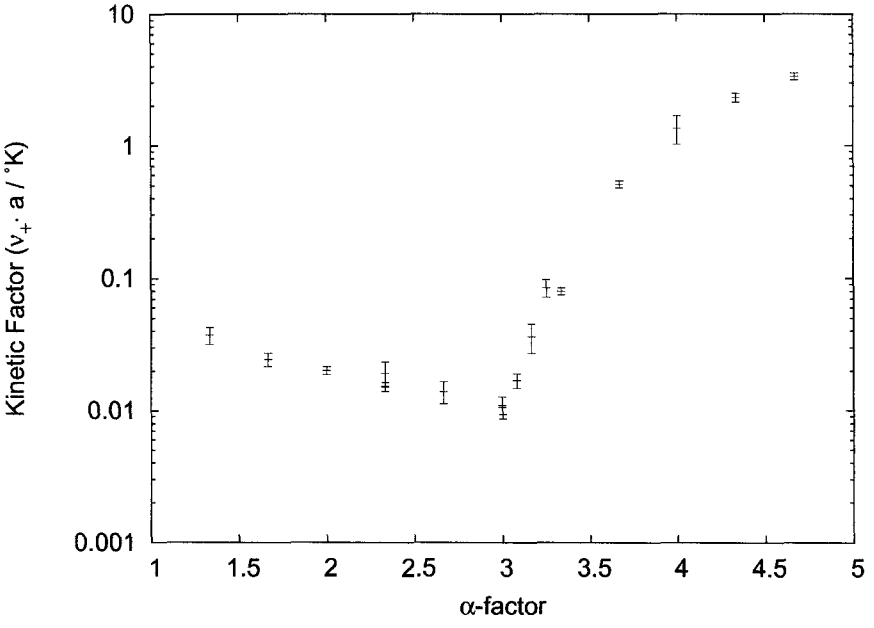

FIGURE 3.3. Kinetics Factor vs α-Factor for a FCC Lattice

This semi-log plot of the kinetic factor vs α-factor shows a distinct discontinuity at $\alpha = 3$. Below the transition the kinetic coefficient decreases logarithmically as a function of α while above the kinetic factor increase exponentially. Error bars on the kinetic factor are the standard deviation of the mean calculated from several time correlations conducted on the simulation of a given α.

α-factor	ΔT (°K / a)	β ($\nu_+ a$/°K)	size of cell (a)	duration ($1 / \nu_+$)
1.333	0.2	0.0371 +/- 0.0055	$50 \times 50 \times 20$	1.832×10^4
1.667	0.2	0.0243 +/- 0.0028	$50 \times 50 \times 20$	3.369×10^4
2.000	0.2	0.0201 +/- 0.0014	$50 \times 50 \times 20$	6.197×10^4
2.333	0.2	0.0192 +/- 0.0039	$50 \times 50 \times 20$	5.699×10^4
2.333	1.0	0.0151 +/- 0.0012	$50 \times 50 \times 20$	5.699×10^4
2.667	0.2	0.0129 +/- 0.0027	$50 \times 50 \times 20$	4.193×10^4
3.000	0.2	0.0110 +/- 0.0017	$50 \times 50 \times 20$	2.468×10^4
3.000	0.2	0.0106 +/- 0.0020	$50 \times 50 \times 20$	1.234×10^5
3.083	0.2	0.0169 +/- 0.0021	$50 \times 50 \times 20$	9.611×10^4
3.167	0.2	0.0361 +/- 0.0089	$50 \times 50 \times 20$	4.678×10^4
3.250	0.2	0.0847 +/- 0.013	$50 \times 50 \times 20$	3.643×10^4
3.333	0.2	0.0796 +/- 0.0045	$50 \times 50 \times 20$	2.270×10^4
3.667	0.2	0.512 +/- 0.031	$50 \times 50 \times 20$	4.175×10^4
4.000	0.2	1.356 +/- 0.33	$50 \times 50 \times 20$	9.216×10^4
4.333	0.2	2.31 +/- 0.18	$50 \times 50 \times 20$	5.650×10^3
4.667	0.2	3.35 +/- 0.20	$50 \times 50 \times 20$	4.158×10^3

TABLE 3.1. Time Correlations of FCC Simulations

α-factor	ΔT (°K / a)	β ($\nu_+ a$/°K)	size of cell (a)	duration ($1 / \nu_+$)
1.000	0.25	1.576 +/- 0.112	$50 \times 50 \times 40$	3.347×10^4
1.667	0.25	0.0609 +/- 0.0039	$50 \times 50 \times 40$	4.925×10^4
2.000	0.15	0.069 +/- 0.014	$110 \times 110 \times 40$	6.223×10^3
2.000	0.25	0.048 +/- 0.011	$85 \times 85 \times 80$	7.468×10^3
2.000	0.15	0.0497 +/- 0.0080	$50 \times 50 \times 40$	1.493×10^4
2.000	0.25	0.0409 +/- 0.0023	$50 \times 50 \times 40$	8.962×10^4
2.333	0.25	0.0302 +/- 0.0024	$50 \times 50 \times 40$	5.436×10^4
2.667	0.25	0.0215 +/- 0.00076	$50 \times 50 \times 40$	5.495×10^5
3.000	0.25	0.0222 +/- 0.0033	$50 \times 50 \times 40$	9.998×10^4
3.333	0.25	0.086 +/- 0.018	$85 \times 85 \times 80$	6.064×10^3
3.667	0.25	0.289 +/- 0.021	$85 \times 85 \times 80$	1.226×10^4
3.667	0.25	0.109 +/- 0.023	$50 \times 50 \times 40$	8.582×10^4
4.00	0.25	0.723 +/- 0.059	$85 \times 85 \times 80$	1.487×10^4

TABLE 3.2. Time Correlations of SC Simulations

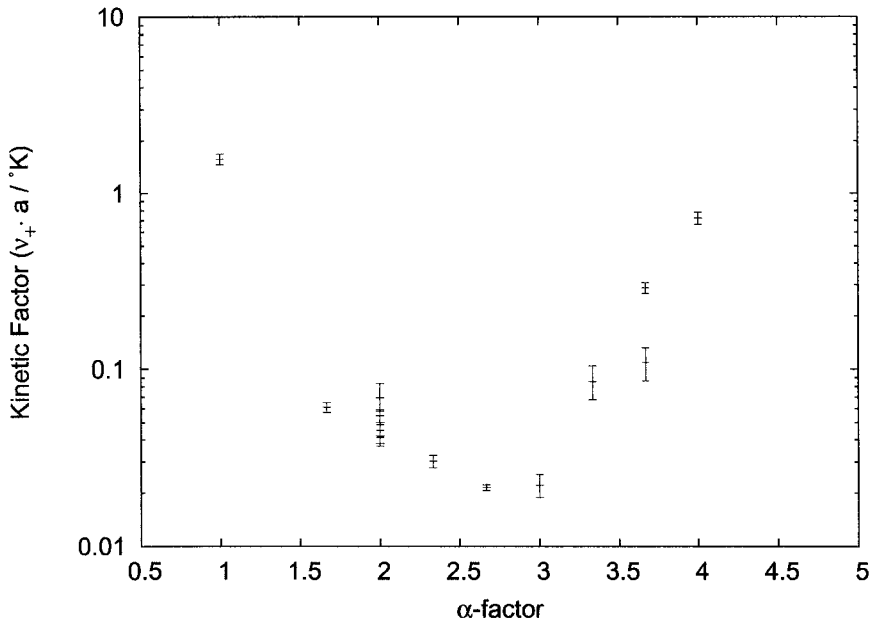

FIGURE 3.4. Kinetics Factor vs α-Factor of SC Lattices

The SC systems exhibit the same behavior as the FCC systems. This includes a shared transition point.

transitions. The first regime exists when the α-factor is small and the development of an interface is energetically unfavorable. As α is increased, an interface between the solid and liquid phases is favorable, however it is rough. This transition is refereed to as the 3D Ising transition, where in a 3D magnetic systems there is no spontaneous magnetization. The surface roughening transition, the second transition seen in the 3D model, may likewise be refereed as the 2D Ising model transition since its behavior is similar to this magnetic phase transition only here it is a 2D transition.

Not only is the surface morphology different in each of these three regimes, but the kinetics changes dramatically as well. It is readily apparent from examining both figures 3.3 and 3.4 that there is an abrupt change in the behavior of the kinetic parameter as a function of α in both the simple cubic systems and the FCC systems. This discontinuity at $\alpha = 3$, as seen in both lattices, is attributed to the surface roughening transition. Figure 3.4

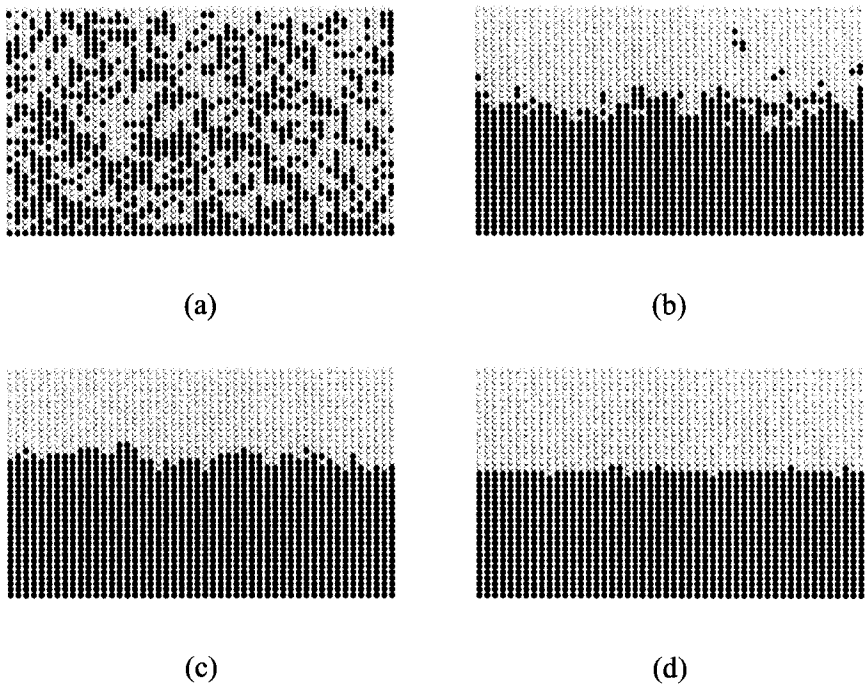

FIGURE 3.5. Surface Roughness

The 3 dimensional Ising lattice gas system exhibits two interface transition points: a 3D transition and a 2D transition. Above the 3D transition, an interface is unfavorable, as shown in figure (a) where $\alpha = 1.0$. In figure (b) and (c) an interface is able to form but is still rough, $\alpha = 1.66$ and 2.33 respectively. Figure (d) shows an interface below the surface roughening transition, or the 2D transition, where $\alpha = 3.66$. These figures are cross-sectional views of a 3D simple cubic lattice. Figures were rendered using Raster3D [77].

shows simulations in all three regimes, while figure 3.4 only shows the surface roughening transition.

The abrupt change of the kinetic factor as a function of α-factor is attributed to the disappearance of the relation pathway that was motivated in the discussion of the kinetic coefficient. It is this pathway which is enabled by the surface presents of a rough surface. The time constants observed in the area where the interface is flat are the faster time constants of arrive of add atoms and the formation rates of kink sites on step edges.

These results not only show this change occurs but it also show the functional depen-

dence of the time constants on the α-factor. It appears that on both sides of the transition the kinetic factor is an exponential function of α.

$$C(\alpha) = A\,exp(-B \cdot \alpha) \tag{3.23}$$

Above the surface roughening transition the FCC lattice system can be fitted with $A = 0.061$ +/- 0.016 and $B = 0.56$ +/- 0.12 for α-factors between 1.33 and 3.00. In the same regime the SC lattice system $A = 0.37$ +/- 0.05 and $B = 1.05$ +/- 0.06. The exponentially behavior of both systems is remarkably similar. This type of behavior is expected since the surface is becoming smoother as α is increase as the number of repeatable step-sites decreases. In this regime the kinetic factor is the kinetic coefficient in equation 3.10.

Below the surface roughening transition the kinetic factor no longer represents the kinetic coefficient. The most significant indication of this is that kinetic factor is displaying a behavior which is contrary to the growth kinetics of the interface. Interfaces below the surface roughening transition grow considerably slower and the growth rate is not linear with under-cooling. Since the measured characteristic times are being influenced by rate of kink site formation, as well as the arrival and departure rates of individual solid atoms, the characteristic times are increasing with increasing α-factor. The relationship between kinetic factor and α may also be fitted with equation 3.23 right above the surface roughening transition. For the FCC lattice system $A = 1.90$ +/- 1.3×10^{-15} and $B = -9.7$ +/- 0.2. While the SC system was fitted with $A = 6.50$ +/- 14.0×10^{-7} $B = -3.5$ +/- 0.6.

Confirmation of the surface roughening transition on the FCC lattice was also sought with the use height-height correlation functions. While this method was originally confusing due to the a misunderstanding of the work of Shugard, Weeks and Gilmer the height-height correlations clearly show that the surface roughening transition occurs between α = 3.0 and 3.1. These results are shown in figure 3.7. The confusion was pertaining to the use of equation 3.3. This function describes the height-height correlation function of a rough interface, however when the interface is smooth the height-height correlation function is very flat with respect to r. When examining the height-height correlation function about

FIGURE 3.6. Simulation Cell

3D view of a typical simulation cell. Cell has dimensions of 50 by 50 by 20 lattice units and in implemented with an α-factor of 3.0 and a ΔT of 0.2 $^{\circ}K/$ lattice unit. Figure was rendered using Raster3D [77].

the surface roughening transition with any lattice gas model this can become confusing since the simulations start with a flat interface where the height-height correlation function is also independent on r and the simulations must be give enough time to come to equilibrium or steady state.

3.4 Conclusion

The application of the fluctuation dissipation therory to a solid-liquid interface has provided significant information about the roughening transition. The time correlation function of the number of solid atoms in a solid-liquid system in a linear thermal gradient exhibits a behavior which decays exponentially in time. By measuring this characteristic time in kMC systems, we have determined the kinetic coefficients of rough interfaces. A strong discontinuity in the kinetic behavior is observed as a function of Jackson's α-factor which

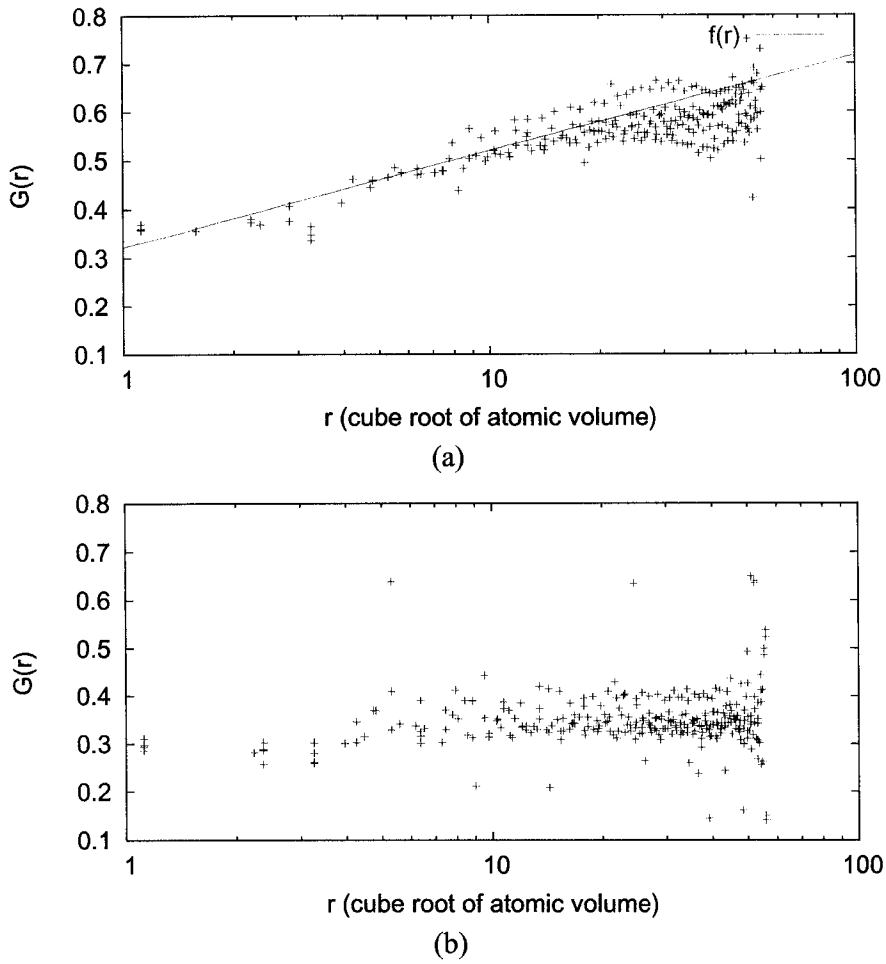

FIGURE 3.7. Height-Height Correlation Function

Figures (a) and (b) show height-height correlation on the $\{100\}$ faces of a FCC lattice. Figure (a) was implemented with $\alpha = 3.0$ while figure (b) was implemented at 3.1. Least squares fit of $f(r)$ of the same form of equation 3.3 resulted in $K_\infty = 0.2683$ and $c = 3.8$. Fit conducted with r in units of the cube root of the atomic volume.

is attributed to the surface roughening transition.

CHAPTER 4

SURFACE ROUGHNESS OF BINARY ALLOY AND IRREGULAR ROD EUTECTICS

4.1 Introduction

Upon examining the rod eutectic system of figure 2.7, it is apparent that the surface roughening behavior of a binary alloy system is different than the roughening behavior of the two pure systems of its components. While the Jackson α-factor expression has been related to the binary crystal-liquid interface [32], there has been some confusion in relating the surface roughening behavior back to the pure systems [45]. Since regular and irregular eutectics are classified by their surface roughening characteristics, understanding the surface roughening behavior of these systems is very important.

This chapter discusses the nature of the surface roughening behavior of binary alloy systems and compares these results to single component systems. These of the surface roughing behavior of a binary alloy have been previously published in the Journal of Crystal Growth [6]. Lastly this chapter will apply knowledge of the surface roughening behavior to irregular rod eutectics.

4.2 Surface Roughness

The surface roughening behavior of single component systems has been previously studied using lattice gas models [92, 33, 101] as discussed in previous chapters. However, the surface roughening behavior of binary systems has received little attention. Binary systems have been studied previously [21, 91, 25] and there growth kinetics can be modeled using the JGT model [3] as detailed in chapters 1 and 2.

The Jackson α-factor has been used as a predictive measure to understand the surface

roughness of a system.

$$\alpha = \left(\frac{L}{k_B T_m}\right)\left(\frac{\eta}{Z}\right) \tag{4.1}$$

The confusion in relating the surface roughness of binary systems to that of single component systems stems from the treatment of the single component system. Since $\Delta S = L/T_m$ the choice of ΔS in single component systems directly controls their surface roughening behavior. The ratio of L/T_m then is used to control the velocity of the interface, noting that $L = Z \cdot \Phi_{SS}/2$. The added complication of a binary system, using the JGT model formulation, changes this arrangement due to the definitions of the parameters in the JGT model.

In the JGT model the entropy differences and bond energies are parameters which are used in the relationship between an ideal solution liquid in contact with a regular solution solid, as shown in equations 2.11, 2.14, and 2.15. The parameter ΔS_A is entropy difference of a single component system of A atoms and it should not be confused with the ΔS of the binary system for various compositions of the liquid phase. A similar statement could be made about the latent heat of fusion of the solid phase however in choosing systems similar to those shown in figure 2.3 this problem is greatly simplified. Here the solid alpha phase solid consists mainly of solid A atoms, and thus the latent heat of fusion is still approximately equal to $(Z \cdot \Phi_{AA}/2)$.

The α-factor then should be calculated using the melting point of the binary system. This equilibrium temperature is the liquidus temperature found on the equilibrium phase diagram.

In order to compare the binary and single component systems a direct measure of the surface roughness needs in to be defined. While rougher surfaces have a higher concentration of repeatable step sites, the density of repeatable step cites an be difficult to calculate. In this study, a definition of surface roughness, $s(t)$, is utilized.

$$s(t) = \frac{N_{SL}(t) - N_{SL}(0)}{N_{SL}(0)} \tag{4.2}$$

This is the same definition used by BCF [15].

Here $N_{SL}(t)$ is the number of solid-liquid bonds on the surface, and $N_{SL}(0)$ is the number of solid-liquid bonds on an atomically smooth surface. In systems where the interface resembles a solid on solid model, where overhangs are not allowed, $s(t)$ is the density of unsatisfied lateral bonds. This measure of surface roughness may be calculated for any state of the JGT model. This measure does not define the location of the surface roughening transition, since the surface roughness increases smoothly through the transition.

Lastly, since the system is at equilibrium, the morphology of the interface is independent of the diffusion rate in the liquid. While choice of the θ, is important in the relaxation of the equilibrium system, it does not effect the measurement of the equilibrium surface roughening.

4.3 Surface Roughness Simulations

The relationship between the surface roughness and the α-factor was examined on the ¡100¿ FCC interface. Simulation were typically conducted with cell dimensions of 200 by 200 by 100 unit cells. Solid-liquid interfaces were then created flat with pure solid of A atoms and a mixture of A and B atoms in the liquid. The evolution of structure of the interface then proceeded at the liquidus temperature of the binary alloy.

This studied utilized three separate phase diagrams with variety of entropies of fusion to examine the binary alloy system. System 1 was run with a ΔS of 7.0 k_B, system 2 with a ΔS of 6.0 k_B and system 3 with a ΔS of 5.0 k_B. For comparison pure systems were also simulated using a similar range of α-factor values. The surface roughnesses as a function of α-factor values is reported in figure 4.1. Rather than using the melting point of the pure material to calculate the α-factor for the alloys, the liquidus temperature of the binary systems was used. The error bars on the data are the standard deviation of the fluctuations of the roughness value around the reported mean. Different α-factors values apply for each point along the liquidus lines of each phase diagram. From figure 4.1 it is

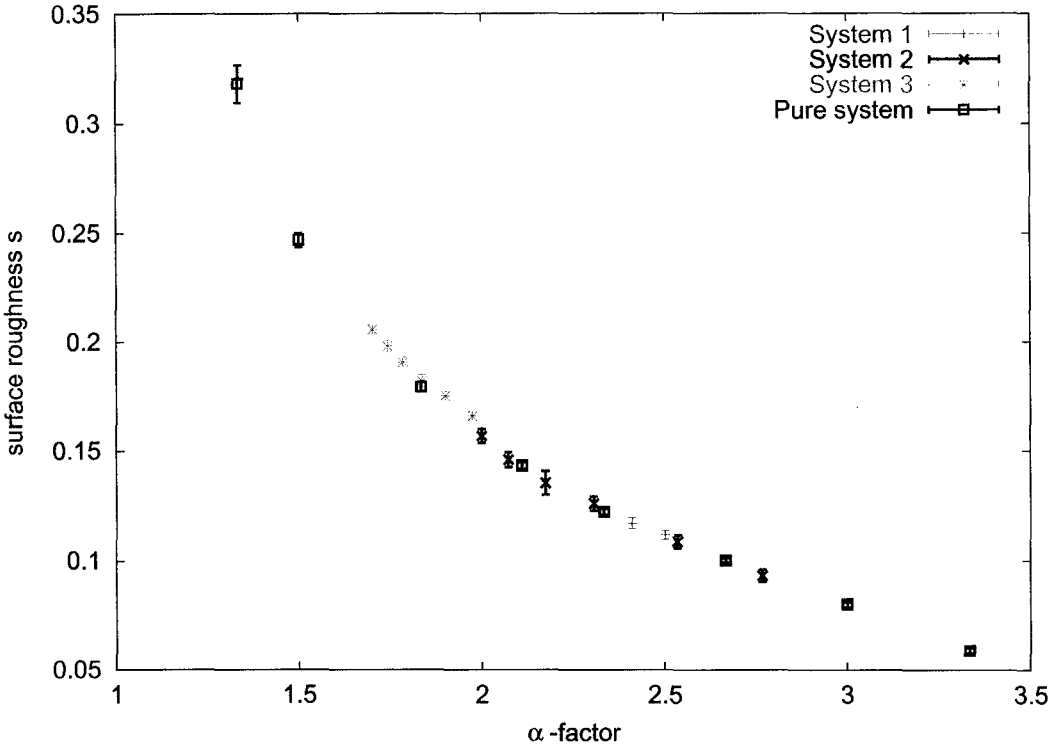

FIGURE 4.1. α-Factor vs. Roughness Parameter

Both binary and pure systems follow the same roughness relationship System 1: $\Delta S_{both} = 7.0k_B, \Phi_{AA} = 1500°K, \Phi_{BB} = 2000°K, \Phi_{AB} = 500°K$ System 2: $\Delta S_{both} = 6.0k_B, \Phi_{AA} = 1470°K, \Phi_{BB} = 2000°K, \Phi_{AB} = 500°K$ System 3: $\Delta S_{both} = 5.0k_B, \Phi_{AA} = 1310°K, \Phi_{BB} = 1800°K, \Phi_{AB} = 500°K$

evident that both pure and binary systems follow the same roughness relationship with a smooth monotonically decreasing roughness with increasing α-factor.

In the case of the simple eutectic system the surface roughness of both phases increases as the system moves to either side of the eutectic. In a rod eutectic system this is more dramatic for the minor phase because of the larger difference between the melting temperature of the pure material and the alloy.

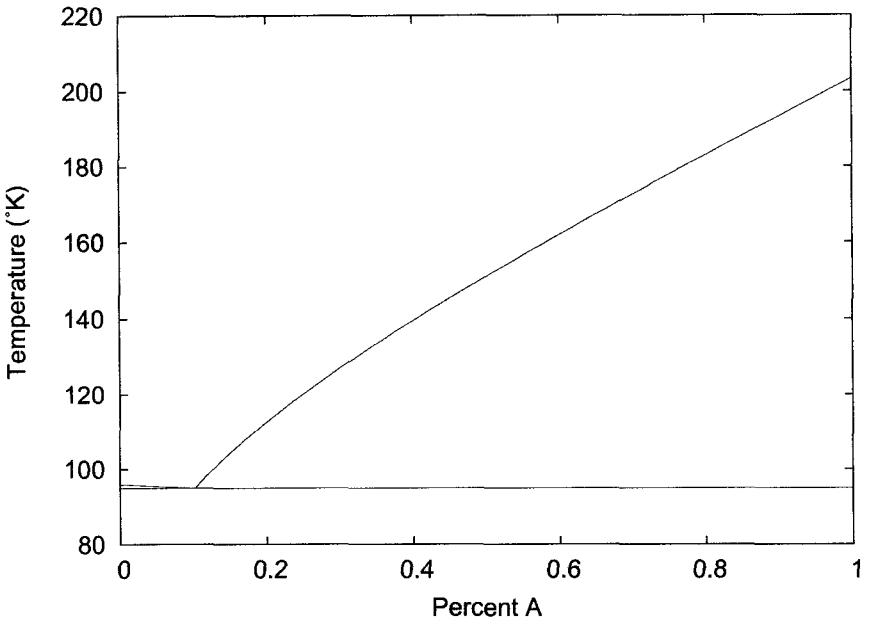

FIGURE 4.2. Irregular Eutectic Phase Diagram

Phase diagram chosen to enable the growth of a irregular rod eutectic system when the major phase is faceted and the minor phase is non-faceted. This phase diagram was calculated using the following parameters with equation 2.22. $\Phi_{AA}/k_B = 67.8°K, \Delta S_A = 2.0k_B, \Phi_{BB}/k_B = 160°K, S\Delta_B = 10.0k_B, \Phi_{AB}/k_B = 40°K, Z = 12$. Solidus lines fall on top of the left and right axes.

4.4 Further Examination of Irregular Eutectics

With knowledge gained from the surface roughening behavior of binary alloys, it is now possible to reexamine the irregular rod eutectic systems. With knowledge of the surface roughening transition of lattice gas models, the original project of systems where the major phase was faceted and the minor phase had a rough interface can continued. An example of one of these systems is displayed in figure 4.2.

The study changed it focus from using a simple cubic lattice to a face centered cubic lattice(FCC) due to the difficulty of directionally solidifying the eutectic system when the faceted interfaced were orient perpendicular to the growth direction. When a simple cubic

lattice who's interface was oriented in the <100> direction was used, the faceted phase would not have time to develop and would be enveloped by the other phase. When faceting occurs out of the plane as in observed in figure 2.7 repeatable step site generation is aided by the solid-solid interfaces and well as the corners of the facets. This choice in geometry was also motivated by the limitations of the existing code. Construction of the initial conditions of rods of A atoms in a matrix of B atoms were forward when conducting simulations a simulation cell with cubic symmetry oriented in the <100> direction. This added complication provided an opportunity to flush out the definition of the definitions of the unit of length both in the simulations as well as interpretation of the J-H model.

The system of figure 4.2 was selected for it surface roughening behavior at the eutectic point where alpha phase has an α-factor of 2.21 for its $\{111\}$ surface and 1.47 for its $\{100\}$ surface. Both of these are above the surface roughening transition of $\alpha_c = 3$. The beta phase of this system at the eutectic point has a α-factor of 5.22 on the $\{111\}$ surface and 3.48 on the $\{100\}$ surface. Both of these interfaces are below the surface roughening transition, thus are smooth. Of both of the beta phase surfaces the $\{111\}$ interface is the smoothest.

Simulations were originally conducted using the J-H model as a guide, as described in chapter 2. Initially a liquid phase 30% richer in the minor component from the eutectic composition was used. This value was latter decreased to 15%. During the course of serval simultions ΔT, r, and θ were modified to produce a stable growing irregular rod eutectic mircostructure. ΔT was increased so that the interface would not remain stationary, while θ was increased when the rod spacing was notably too small. In systems where the rod spacing was too small the rod structure would breakup by nucleating new rods in the middle of the major phase. The scale of this new rod structure provided a hint on the dimensions of the simulations cell that would support stable rod growth. The last modification was to the rod spacing when the rod spacing was only slightly off. The parameters for the final rod eutectic system are found in table 4.1 and views of the simulation cell are shown in figures 4.3 and 4.4.

Input Parameters		Intermediates		Final Parameters	
Φ_{AA}	67.8 $k_B \cdot {}^\circ K$	a_α	1.994 a	$2\,m\,a^R$	58.82 $^\circ K \cdot a$
Φ_{BB}	160 $k_B \cdot {}^\circ K$	a_β	43.02 a		
Φ_{AB}	40 $k_B \cdot {}^\circ K$	a^R	2.929 a		
ΔS_A	2.0 k_B				
ΔS_B	10.0 k_B				
m_α	214.4 $^\circ K$	m	10.04 $^\circ K$		
m_β	10.53 $^\circ K$	θ_α	2.41°		
T_e	94.98 $^\circ K$	θ_β	65.0°		
Z	12				
ζ	9	M	0.0395		
ρ(assume)	1				
				$\theta_{proposed}$	62.19
ΔT	2.98 $^\circ K$	r	4.98 lattice units	θ_{used}	75
R_{cell}	30 lattice units	R_{J-H}	25.00 a	$\Delta T \cdot R_{J-H}$	74.51 $^\circ K \cdot a$
C_{liq}	11.5% A atoms				

$a = 0.630$ lattice units, for a FCC lattice.
(note: $a = \sqrt[3]{atomic\,volume}$)

TABLE 4.1. Stable Rod System

In this table R_{cell} is the size of the simulation cell as defined in figure 2.4 and R_{J-H} is the R parameter found in the J-H model.

As with the irregular eutectic of table 2.2, this eutectic system also diverges from the J-H model. However here, the calculated rod spacing is roughly twice as small as the one in the simulation. This result requires further evaluation of both types of irregular rod eutectics to see if this pattern really holds for more than three systems. These systems also need to be examined with diffusion rates more closely resembling the J-H model.

4.5 Conclusions

The surface roughness of a binary solution follows the same behavior as pure systems in relation to the α-factor when the liquidus temperature is used for the melting point of the

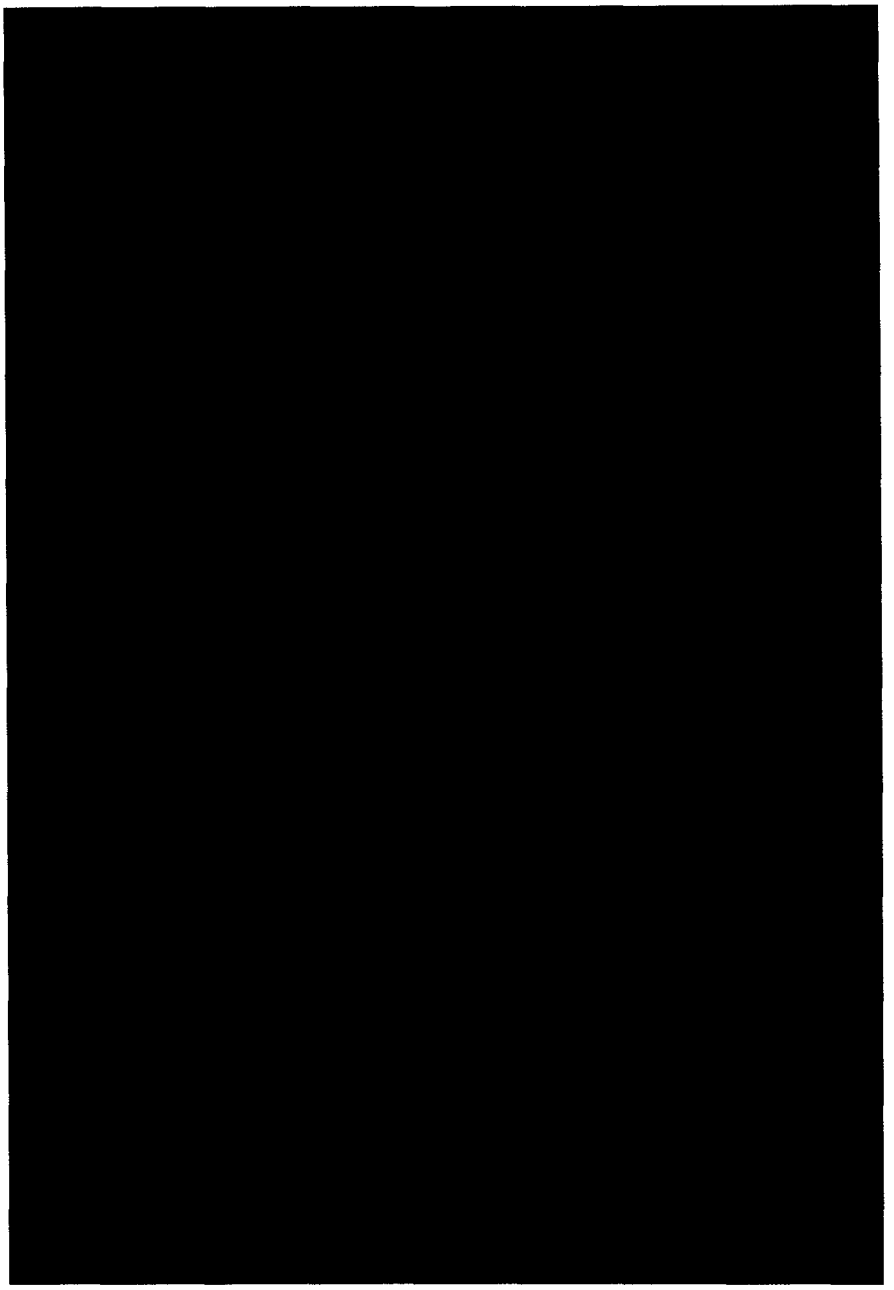

FIGURE 4.3. Irregular Rod Eutectic 3D View

Stable rod eutectic growth using parameters shown in table 4.1. Simulations were conducted on a FCC lattice oriented in the $\{100\}$ direction on a simulation cell with dimensions of 30 by 52 by 175 unit cells. The liquid composition (C_{liq}) was 11.5% minor component. Figure was rendered using Raster3D [77].

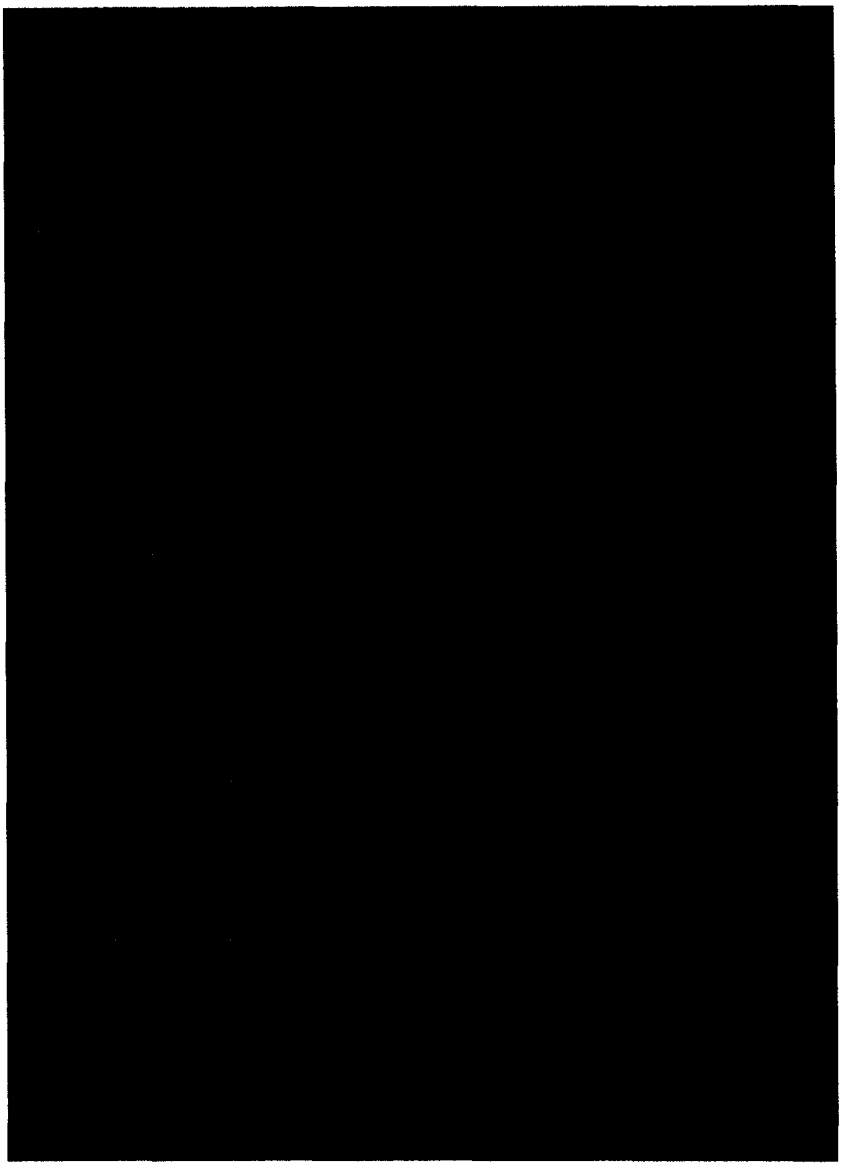

FIGURE 4.4. Irregular Rod Eutectic 2D View

Diagonal cross-section of figure 4.3. Both liquid and solid atoms are displayed in figure. Early behavior of the alpha phase rod due initial conditions of the interface.(flat interface) Figure was rendered using Raster3D [77].

system. Thus, the surface roughening behavior in an eutectic system does not depend on the entropy of fusion of the pure components rather it depends on the latents heats of the two phases and the eutectic temperature. In particular this means that the interfaces of the two alloy systems will be smoother than the interfaces of the isolated systems of the pure materials.

These observations have been used to develop stable rod growth of an irregular eutectic system using the spin one Ising lattice gas model. Like experimentally observed irregular eutectic systems, these rods have also deviated from the expected rod spacings of the Jackson-Hunt model.

CHAPTER 5

DISLOCATION ETCH-PIT SIMULATIONS

5.1 Introduction

Chemical mechanical polishing (CMP) is now widely used in the semiconductor industry [93]. CMP, stress corrosion cracking and dislocation etches share the common feature in that the rate of chemical attack depends on the local stress level. In both CMP and stress corrosion cracking the combined effect of chemical attack and mechanical stress is an order of magnitude greater than either acting alone. In this project, we have modeled the formation of dislocation etch pits by using kinetic Monte Carlo (kMC) simulations in order to study the interaction of stress on the etching process.

Dislocation etches have been used extensively to evaluate the perfection of crystals. [26, 72, 50, 61, 78] The impact of localized stresses on growth and dissolution kinetics has been of great interest for a long time [94]. One of the first examinations on the effects of dislocations on dissolution was conducted by Cabrera and Levine [16]. By extending the BCF [15] model of crystal growth through screw dislocation to dissolution they applied spiral step edge kinetics to the dissolution of crystals [16]. While this model does include the stress fields associated with a screw dislocation, etch pits formed by this mechanism are always shallow. This is the case since this model examines a stress single step edge and continuous step edge would lead to shallow pitting. Dislocation pitting and dislocation coring was also examined by Frank [36], where he showed deeps pit can also be formed at equilibrium conditions at the center of the dislocations due to the high stresses [36]. The dynamics of the hollow dislocation cores have been examined using lattice models [42]. In the model implemented by Guang-Zhao et. al., the hollowing of the dislocation core was examined on a simple cubic lattice where the events of atoms arriving and departing the solid interface where chosen by a non-random process. In their alogoritham events that were the most

probable occurs first. An Analytic solution to this model was constructed for the case of rough surfaces where crystallographic effects are inconsequential [34]. Dislocation etching studies have also examined etching processes on diamond cubic [102, 101, 24].

This study focuses on the effects of stress rather than lattice geometry around a dislocation and examines with the same model both faceted and non-faceted etch pits. Here we examine the effects of etching rates and dislocation strengths on the formation of etch-pits. This modelalos produces both faceted and non-faceted etch-pits. This work has been previously presented in the Fall 2001 Materials Research Society Meeting [7].

5.2 Simulation Description

A kinetic Monte Carlo (kMC) algorithm was implemented to simulate dislocation etching on a silicon surface. The dislocation is assumed to be straight and perpendicular to the surface. Atoms are irreversibly removed from the lattice at random with a weighted probability depending on the number of nearest neighbors as well as their physical location in the lattice. This probability is expressed as in the rate expression:

$$\nu_{-} = \nu_o e^{-n(\phi - E(n,r))} \tag{5.1}$$

Here ν_{-} is the frequency with which atoms are removed from the solid while ν_o is a pre-exponential factor. E is the geometric energy representing a weakening of the bonds. The strength of the unstressed bond in the etching solution is represented by ϕ. n is the number of nearest neighbor solid atoms and r is the distance from the center of the dislocation. At the interface the concentration of the etchant is uniform, and the atoms which are in contact with the solution are the only ones removed.

This model treats the dislocation purely as a source of stress on the lattice, and ignores the changes in local geometry of the lattice due to the dislocation. For a dislocation with a Burgers vector perpendicular to the surface, as with a pure screw dislocation, the stress on the bonds is independent of the detailed configuration of the atoms at the core and is

only dependent on the distance from the dislocation core. The stress field has cylindrical symmetry about the line of the dislocation [79]. In order to avoid the singularity at the center of the dislocation core, atoms positioned there are assumed to feel the same stress energy as their nearest neighbors. This stress will be interpreted in terms of the bond energy as

$$E(n,r) = \begin{cases} \frac{E_n}{r} & 1 < n < Z \\ 0 & 1 \geq n \geq Z \end{cases} \tag{5.2}$$

The code for the kMC stores the lattice as an array of structures. Each atom in the lattice stores the location of its nearest neighbors as well as any events that may occur for that lattice site. The data structure is also responsible for holding the value of the geometric energy since E_n/r is constant for each lattice site. Simulations are conducted on a three dimensional lattice. During the course of the simulation the program outputs the full lattice in real coordinates that may be viewed using a rendering program. [77] (see Figure 5.1) Time in these simulations has been kept as a relative parameter which mainly depends on the choice of ν_o. Here ν_o was set to equal to one.

5.3 Simulations

Simulations were typically conducted on a diamond cubic lattice 125 by 125 by 200 unit cells in size. The lattice was oriented with its $\{100\}$ plane in contact with the etchant. The etching strength and geometric energy values, ϕ and E_n, were chosen such that the pit's formation was not impacted by the boundaries of the simulation cell. In this study, ϕ ranged from one to nine and E_n ranged from 0.1 to 0.8. In this range, it is possible to examine both faceted and non-faceted etch-pits, and shallow and deep pits.

Pits in these simulations are observed to etch at a uniform rate. Both the center of the pit and areas outside the pits mouth etch at rates which are linear with respect to the log of both the ϕ's and E_n's. These pits also exhibited well defined boundaries. Thus, material outside the pit was not being affected by the geometric potential. Figure 5.1 is the result of a typical simulation.

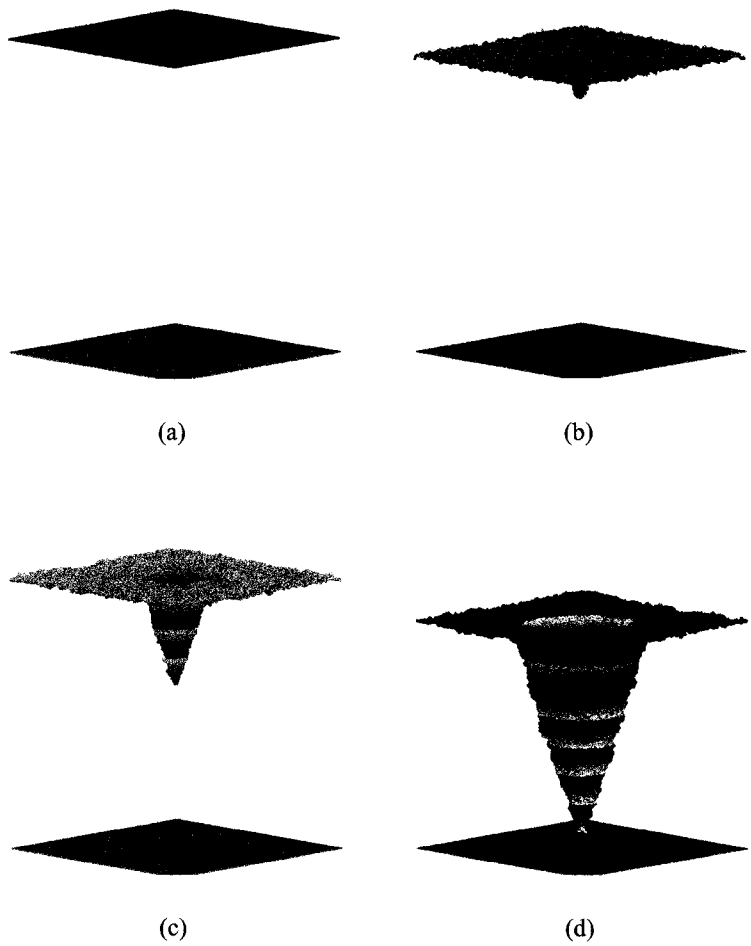

FIGURE 5.1. Time Evolution of Etch-Pit Simulation

Only the interface atoms are shown in this figure. Banding with period of 16 unit cells is included to indicate the depth of the pit. Simulation is conducted with $\phi = 2$, $E_n = 0.3$ unit cells and $\nu_o = 1$. (a) t = 0, (b) t = 200,(c) t = 450, (d) t = 900 (time in arbitrary units). Figures were rendered using Raster3D [77].

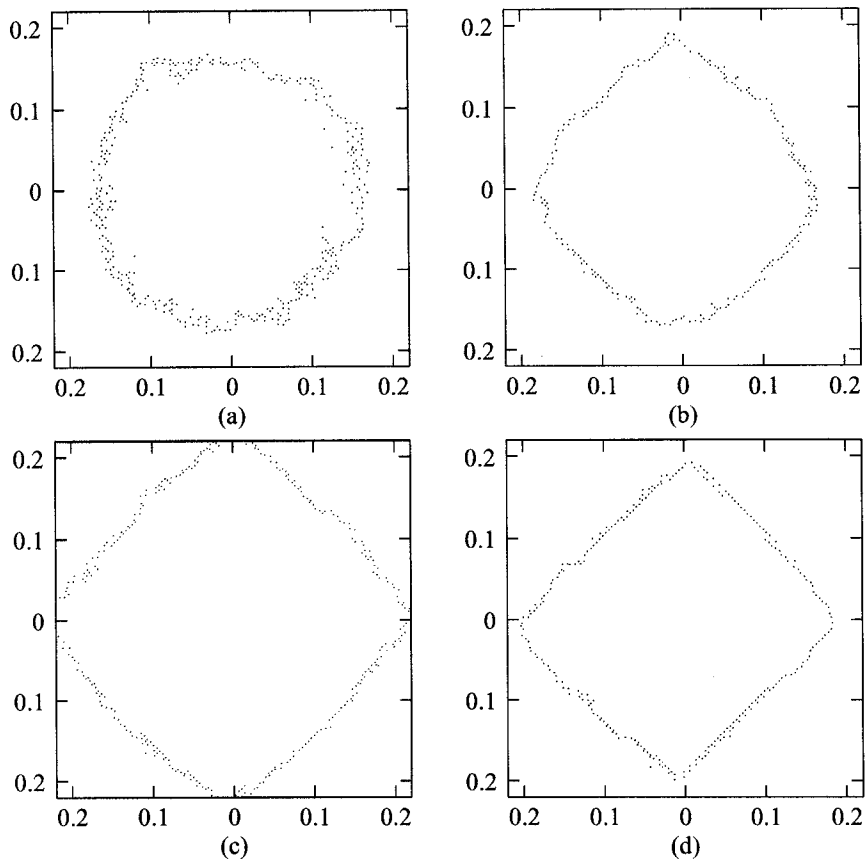

FIGURE 5.2. Pit Cross Sections

Interface atoms located in a plane at the middle of the etch pit perpendicular to the dislocation line (a) $\phi = 1$, $E_n = 0.5$ (b) $\phi = 5$, $E_n = 0.5$ (c) $\phi = 7$, $E_n = 0.5$ (d) $\phi = 9$,$E_n = 0.6$ E_n is in unit cell units.

The ϕ dependence on the pit formation can be seen in Figure 5.2. This figure displays only the interface atoms located in a plane at the middle of the etch pit perpendicular to the dislocation line. At low values of ϕ the etch is non-crystalgraphic. The cross sections are independent of the lattice symmetry and are circular. As the ϕ values increase the pit reflects the symmetry of the crystal, thus when ϕ is equal to nine the etch-pit cross section is nearly a square. It should also be noted that as the ϕ increases the surface becomes smoother.

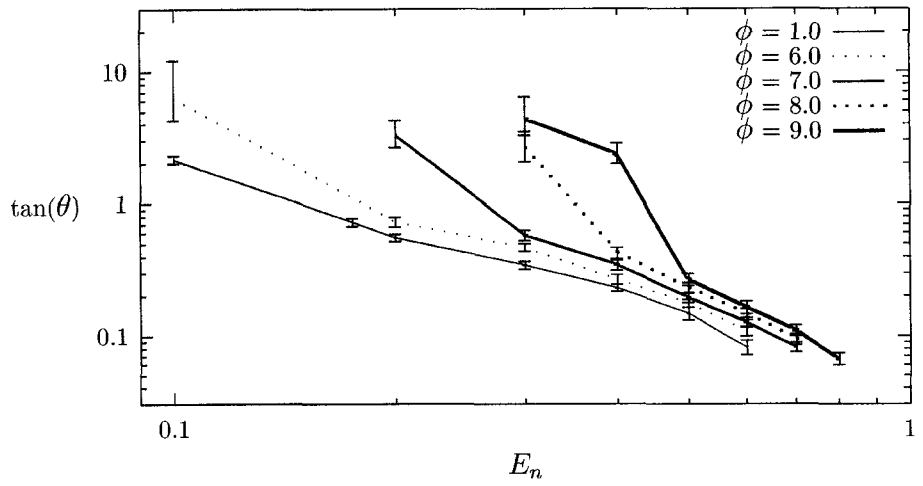

FIGURE 5.3. Etch-Pit Angle vs. E_n

Etch pit angle is the average polar angle measured at the bottom of pit from the dislocation line to a mid-point surface atom.

The geometric energy, E_n, impacts the etch rate of the pit and pit sharpness increases as E_n increases. This has been quantified by measuring the polar angle from the bottom of the pit to mid-pit atoms, θ. During the course of the simulation, θ approaches a constant value. These values are plotted as the log of the tangent of θ against the log of E_n in Figure 5.3 for various values of ϕ. The tangent of θ is the aspect ratio of the etch-pit. While ϕ does play a part in determining the aspect ratio of the etch-pit, the etch-pit is far more sensitive to the geometric energy. The data displayed in this figure exhibits more scatter since shallow pits are not well formed thus there is a larger spread in the values of the polar angles.

5.4 Conclusions

With a simple model of the stresses around a dislocation we have been able to duplicate the shape of experimentally observed dislocation etch-pits. By varying two parameters, etch strength and geometric energy, we have been able to produce both shallow and deep

dislocation etch-pits as well as crystallographic and non-crystallographic pits.

CHAPTER 6

STRESSED STEP SIMULATIONS

6.1 Introduction

A local stress can play a significant role in crystal dissolution. The effect is evident in chemical mechanical polishing where etching rates of solvent solutions are dramatically increased by localized stresses. The origin of this interaction between mechanical stress and chemical dissolution has been somewhat of a mystery. It is my believe that the present results shed some light on this interaction. Direct observations with an AFM probe tip on a calcite surface have shown increased dissolution rates with increased tip pressure [83]. Step edges were observed to recede away from the tip in near equilibrium solutions using contact forces around 200 nN.

To examine this behavior a kinetic Monte Carlo (kMC) study of the effects an AFM probe tip interacting with a crystal step edge has been conducted. This lattice gas model incorporates a local stress field, in the form of a geometrically dependent bond energy perturbation, into a spin 1/2 Ising model treatment of stepped solid-liquid interface. The goal of this research is to attempt to reproduce the effects of an AFM probe tip in the vicinity of a step edge and thus gain an understanding of the effects of local stresses on growth and dissolution processes. This work has been previously published in the Journal of Crystal Growth [5].

6.2 Kinetic Monte Carlo

The kMC model implemented for this study is similar to previous work [7]. A step is introduced into the surface by using periodic boundary conditions in the$\{001\}$ direction while periodic boundary conditions in the $\{010\}$ direction are offset one lattice spacing [70, 38]. Simulations start with a flat interface oriented in the $\{1n0\}$ direction where n is the

size of the simulation cell in the $\{010\}$ direction. Simulations are typically conducted with a simulation cell containing 125 by 125 by 20 atoms with 10 initial solid layers.

The interface then evolves with a kMC implementation of a spin 1/2 Ising type model where liquid atoms join the solid at a rate of:

$$\nu_i^{LS} = \nu_o exp\left(-\frac{\Delta S}{k_B}\right) \tag{6.1}$$

where ΔS is the entropy difference between the solid and liquid phases, ν_o is a pre-exponential factor, and k_B is the Boltzmann's constant. Atoms are removed from the solid surface to join the liquid at a rate of:

$$\nu_i^{SL} = \nu_o exp\left(-\frac{n_i^{sol}\left(\Phi_{ss} - E_{geo}\left(r_i\right)\right)}{k_B T}\right) \tag{6.2}$$

where Φ_{ss} is the solid-solid bond energy, n_i^{sol} is the number of solid nearest neighbor atoms around the i^{th} atom, T is the temperature of the simulation and $E_{geo}(r_i)$ the position dependent bond perturbation. To approximate the stress effect produced by the AFM tip on the crystal surface a static Gaussian stress field centered in the middle of the simulation cell was used.

$$E_{geo}(r) = \alpha e^{-(\beta r)^2} \tag{6.3}$$

Here r is the distance, in cylindrical coordinates, away from the center of the simulation cell, and α and β are the parameters which control the magnitude of the perturbation. This stress field was chosen since it is a radially symmetric smooth function which is close to parabolic at $r = 0$ and approaches zero at $r \rightarrow \infty$. To examine the pressure dependence of a single probe tip on the surface, α was modulated while keeping the curvature, (s), at $r = 0$ of the stress field constant.

$$s = \frac{1}{2\alpha\beta^2} \tag{6.4}$$

The curvature of the potential field was chosen to impact the development of the step edge but not to halt step edge development. This was typically done with a curvature of 4000 lattice units. A typical stress field is shown in figure 6.1.

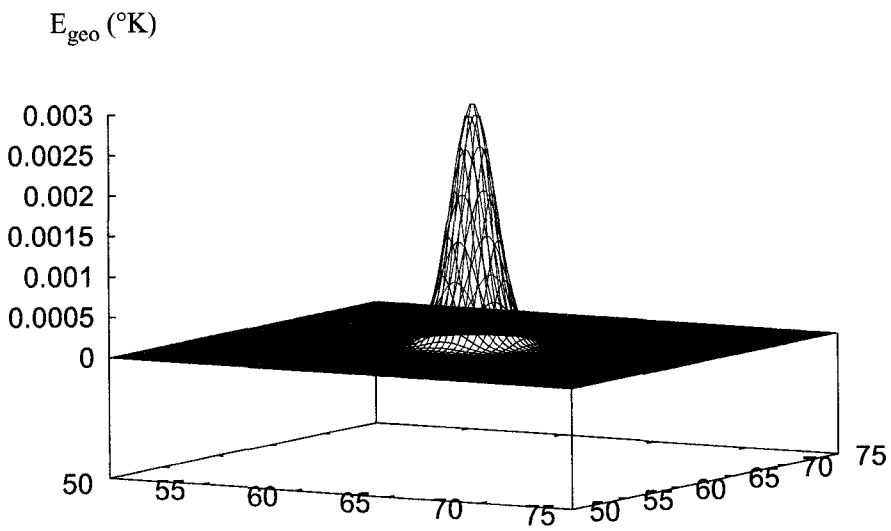

FIGURE 6.1. Stress Field

Figure shows the stress field imposed on the simulation cell. X and Y axes are the coordinates in the simulation cell. $\alpha/k_B = 0.003$ °K and $\beta = 0.2041$ 1/Au.

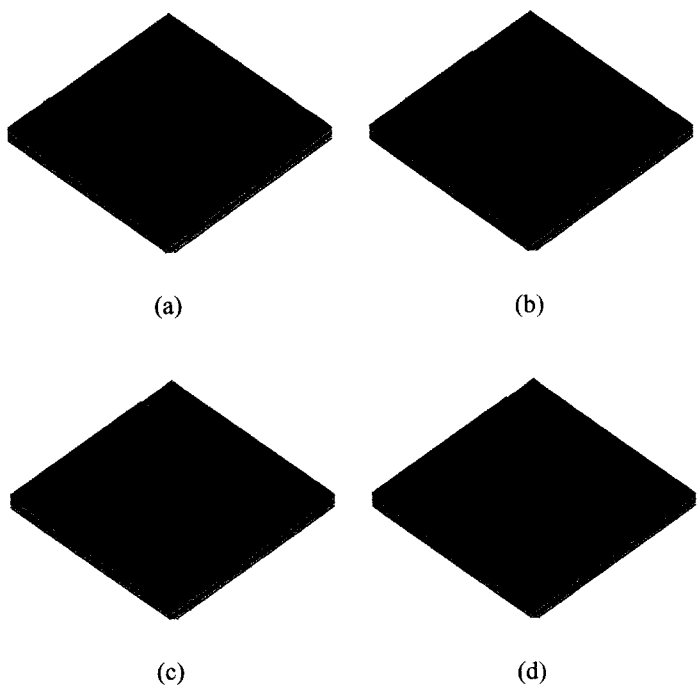

FIGURE 6.2. Time Evolution of Stressed Step Edge

Figures display the time evolution of a typical stressed step simulation. It was conducted at $T = 99.50$ °K with $\Phi/k_B = 500$ °K, $\Delta S/k_B = 15.0$, $\alpha/k_B = 0.0030$ °K and $\beta = 0.2041$ 1/Au. (a) t = 5, (b) t = 11,(c) t = 17, (d) t = 18 (time in arbitrary units). Figures were rendered using Raster3D [77].

6.3 Simulations / Results

Given this model there are three parameters that need to be examined to compare my results to laboratory observations; these are the kink site density, the velocity of the interface and the pressure of the AFM tip. These parameters are controlled with the choice of ΔS, the under-cooling of the interface (ΔT) and, the strength of the perturbation α. ΔT is defined as:

$$\Delta T = T_m - T = \frac{3\Phi_{ss}}{\Delta S} - T \tag{6.5}$$

for a simple cubic lattice. Here T_m is the melting point of system. In this study T_m was set to 100 °K. The magnitude of the bond strength Φ_{ss} is dependent on the choice of ΔS as given by the relation:

$$\frac{\Delta S}{k_B} = \frac{L}{k_B T_m} = \frac{\Phi ss}{3 k_B T_m} \tag{6.6}$$

With small ΔT's, the kink site density is only dependent on ΔS. To maintain well defined step edges, simulations were conducted below the surface roughening transition on the $\{100\}$ interface [49]. Simulations with $\Delta S/k_B$ ranging from 7 to 17 were conducted. Velocity of the step-edge was then controlled by the amount of under-cooling of the system.

Then stress fields, which were large enough so that growing or receding step edges were perturbed, yet were small enough so that there is no spontaneous pit formation in a flat plane at the center of the simulation cell were applied. This range of potential fields (α) is dependent on ΔT and ΔS. At ΔT = 1 °K and $\Delta S/k_B$ = 9 this range of α/k_B's was 0.0025 to 0.0015 °K while with $\Delta S/k_B$ = 15 at the same ΔT is from 0.003 to 0.004 °K. A typical simulation is shown in figure 6.2.

Significant differences in the interaction between advancing and retreating step fronts with the potential field were observed. Advancing step edges are impeded by the stress field as seen in figure 6.2. The growth rate of the crystal slows, and the step edge becomes rougher while the step edge is being influenced by the applied potential field. When the outer part of step proceeds far enough way from the center region of the perturbation the

center part of the step snaps away from the imposed field. The distance that the unperturbed part of the step travels before this snap occurs increased with decreasing ΔS.

Growth simulations were conducted so that the step edge would be influenced by the field, but not completely stopped. Step edges that were stopped by the stress field were overly influenced by the nature of the periodic boundary conditions. The amount of undercooling also had an effect on the ability of the field to stop the progress of the step edge. With a fixed simulation size, the critical field strength to stop a growing step edge decreased with speed of the growing step edge. Receding step edges were not dramatically effected by the stress field. Stress fields strong enough to effect the receding step typically were strong enough to produce pit formation on the flat interface.

6.4 Discussion

The concept that AFM tip is in contact with the surface is misleading. The AFM tip interacts with the surface mainly though van der Waals forces. The attractive potential between an atom a distance D away from the surface of a sphere of radius R interacting with the attractive part of the van der Waals potential of $w(r) = -C/r^6$ may be written as

$$W(D) \approx \frac{\pi C \rho}{6D^3}\left(1 - \frac{3}{2\left(1+\frac{R}{D}\right)}\right) \tag{6.7}$$

where $R \gg D$. Here, ρ is the number density atoms in the sphere, and C is the Hamaker constant of the medium between the atom and the sphere [48]. Assuming a Si_3N_4 AFM tip with a radius of curvature of $40nm$ at a distance of $1\ nm$ away from the surface, the atoms closest to the tip would be affected by a $7.5 \times 10^{-22} J/Au^2$ potential field. This value was calculated using the Hamaker constant for water of $1.4 \times 10^{-77} Jm^6$ and the atom density of Si_3N_4 of $\rho = 9.9 \times 10^{28} atoms/m^3$.

The dissolution process of calcite is not as simple as this kMC model. [27] However using approximate bond energies calculated using molecular dynamics of a hydrated surface of calcite, the probe tip would have an effect 0.005 times as strong as the bond energy. It

has been observed that perturbations of this magnitude are capable of reproducing experimentally observed phenomena.

6.5 Conclusions

A lattice gas model which reproduces the results observed in high contact pressure AFM studies has been developed. This model has shown that bond energy perturbations necessary to deform a step edge are of the same magnitude of van der Waals attraction between a sphere located at AFM type distances. A clear difference in the growth and dissolution step interaction with the potential field which is attributed to ability of the step to pass though this perturbation has been seen.

These results have significant impact on the understanding of the mechanism for chemical mechanical polishing. The results demonstrate that the attractive part of the interaction potential between the probe tip and the substrate can increase the rate at which atoms leave the surface. Similarly, a particle near a surface in a chemical etching solution can increase the local rate of chemical attack. This is unlike the notion that material is removed from the surface mechanically by the particles, which would involve the repulsive part of the interaction potential. This suggests that the particles present in the slurries used for chemical mechanical polishing may not, in fact, mechanically remove material. But, rather, they enhance the local dissolution rate when a particle is near the surface. This increases the rate of chemical removal of material, without the usual surface roughening associated with purely chemical attack, so that a highly polished surface can be obtained rapidly.

CHAPTER 7
CONCLUSIONS

Kinetic Monte Carlo studies have been conducted for two main topic areas in order to gain a deeper understanding into their fundamental behavior. These topic areas are, irregular rod eutectics and chemical mechanical polishing. The lattice gas model, with nearest neighbor interactions, has provided a platform capable of maintaining the critical atomistic effects observed in real systems. These effects are evident in the anisotropy of surface tensions and interface kinetics of smooth interfaces.

For the rod eutectic project, a method has been developed to examine the directionally solidified rod eutectic structure. These structures have been examined with the JGT lattice gas model, which is similar in nature to the Ising spin model. Since this system properly handles interface kinetics above and below the surface roughening transition, it has been possible to examine both the regular and irregular eutectic structures. This is of particular importance since while the regular eutectic structure are relatively well understood, through the application of the Jackson-Hunt model, irregular eutectic structures have remained elusive because of their complex interface kinetics.

During the course of this project a unique approach to discerning the surface roughening transition of a lattice gas system, utilizing fluctuation dissipation theory, has been implemented. This study has shown that the interface kinetics, as measured using time correlations on systems fluctuating about equilibrium, changes abruptly at the surface roughening transition.

In applying this knowledge to the eutectic system, the relationship between surface roughening characteristics of a binary solution and that of a single component system needed to be explored. It has been demonstrated that the surface roughening behavior of a binary system is similar to that of a single component system with respect to the Jackson-α

factor if the liquidus temperature of the binary system is used as the melting temperature of that system. With the knowledge of from these studies, simulations of irregular rod eutectic systems have been conducted, where the major phase was faceted and the minor phase was smooth. While there is a great deal of work that still should be done on evaluating the stability of rod eutectic growth with kMC, this dissertation has shown the power a simple lattice gas model to study the development of the mircostructure of these alloys.

The second part of this dissertation has focused on examining the effects of localized stresses in lattice gas models with the goal of increasing our understanding of chemical mechanical polishing. A study of dislocation etch-pitting has shown that the atomistic kMC model can examine the full continuum of etch-pits from those with high symmetry where the underlying lattice does not affect the morphology of the etch-pit to those etch-pits which are highly influenced by the underlying lattice. This modeling was done by examining bond strengths and modifying the strength of chemical attack. A study of the effects of an AFM tip on the motion of an isolated step edge has demonstrated that step pinning, as observed in laboratory studies, can be reproduced by the use of a lattice gas model with the application of energy perturbations which are of the order of magnitude of van der Waals forces. The results of these simulations suggest a new approach to modeling the mechanical effects in chemical mechanical polishing where the particles through their interaction with the surface are weaken the bonds in the surface make them more susceptible to chemical attack.

REFERENCES

[1] AKAMATSU, S., PLAPP, M., FAIVRE, G., AND KARMA, A. Pattern stability and trijunction motion in eutectic solidification. *Physical Review E 66* (2002), 030501.

[2] BASKARAN, V., AND WILCOX, W. R. Influence of convection on lamellar spacing of eutectics. *Journal of Crystal Growth 67* (1984), 343–352.

[3] BEATTY, K. M. *Simulations of Binary Alloy Solidifcation*. Ph. D., University of Arizona, 1997.

[4] BENTZ, D., BETUSH, W., AND JACKSON, K. Kinetic monte carlo simulations of rod eutectic growth; the surface roughening transition of binary alloys. In *2002 Materials Science Conference* (June 25-26 2002), Materials Science Discipline Work Group, NASA. .

[5] BENTZ, D. N., BETUSH, W. J., AND JACKSON, K. A. The effect of stress fields from a probe tip on step motion using kinetics, monte carlo. *Journal of Crystal Growth 250*, 1-2 (2003), 166–169.

[6] BENTZ, D. N., BETUSH, W. J., AND JACKSON, K. A. Kinetic monte carlo simulations of the surface roughening of binary systems. *Journal of Crystal Growth 250*, 1-2 (2003), 162–165.

[7] BENTZ, D. N., AND JACKSON, K. A. Kinetic monte carlo simulations of dislocation etch-pits. In *Surface Engineering 2001 Fundamentals and Applications* (November 2002), W. J. Meng, A. Kermar, G. L. Doll, Y. T. Cheng, S. Veprek, and T. W. Chung, Eds., vol. 687, Materials Research Society, pp. 41–46.

[8] BINDER, K. Applications of monte carlo methods to statistical physics. *Reports on Progress in Physics 60*, 5 (1997), 487–559.

[9] BINDER, K., AND HEERMANN, D. W. *Monte Carlo Simulation in Statistical Physics: an Introduction*, 4th ed. Springer series in solid-state sciences. Springer, Berlin; New York, 2002.

[10] BLUE, J. L., BEICHL, I., AND SULLIVAN, F. Faster monte carlo simulations. *Physical Review E (Statistical Physics, Plasmas, Fluids, and Related Interdisciplinary Topics) 51*, 2 (1995), R867–8.

[11] BORTZ, A., LEBOWITZ, J., AND KALOS, M. A new algorithm for monte carlo simulation of ising spin systems. *Journal of Computational Physics 17*, 1 (1975), 10–18.

[12] BRIELS, W. J., AND TEPPER, H. L. Crystal growth of the lennard-jones (100) surface by means of equilibrium and nonequilibrium molecular dynamics. *Physical Review Letters 79*, 25 (December 1997), 5074–5077.

[13] BROUGHTON, J. Q., GILMER, G. H., AND JACKSON, K. A. Crystallization rates of a lennard-jones liquid. *Physical Review Letters* (1982).

[14] BURDEN, M. H., AND HUNT, J. D. The extent of the eutectic range. *Journal of Crystal Growth 22* (1974), 328–330.

[15] BURTON, W. K., CABRERA, N., AND FRANK, F. C. The growth of crystals and the equilibrium structure of their surfaces. *Philosophical Transactions of the Royal Society of London 243*, 866 (June 1951), 299–358.

[16] CABRERA, N., AND LEVINE, M. M. On the dislocation therory of evaporation of crystals. *Philosophical Magazine 8*, 5 (May 1956), 450–458.

[17] CALLEN, H. B., AND WELTON, T. A. Irreversibilty and generalized noise. *Physical Review 83*, 1 (July 1951), 34–40.

[18] CARAM, R., BANAN, M., AND WILCOX, W. R. Directional solidification of pb-sn eutectic with vibration. *Journal of Crystal Growth 114* (1991), 249–254.

[19] CARAM, R., CHANDRASEKHAR, S., AND WILCOX, W. R. Influence of convection on rod spacing of eutectics. *Journal of Crystal Growth 106* (1990), 294–302.

[20] CHANDLER, D. *Introduction to Modern Statistical Mechanics*. Oxford University Press, New York, 1987.

[21] CHERNOV, A. A., AND LEWIS, J. Computer modeling of crystallization of binary systems; kinetic phase transitions. *Journal of Physics and Chemistry of Solids 28*, 11 (November 1967), 2185–2190.

[22] CHUI, S., AND WEEKS, J. Dynamics of the roughening transition. *Physical Review Letters 40*, 12 (1978), 733–736.

[23] CORIELL, S. R., MCFADDEN, G. B., MITCHELL, W. F., MURRAY, B. T., ANDREWS, J. B., AND ARIKAWA, Y. Effect of flow due to density change on eutectic growth. *Journal of Crystal Growth 224* (2001), 145–154.

[24] CUPPEN, H., VAN VEENENDAAL, E., VAN SUCHTELEN, J., VAN ENCKEVORT, W., AND VLIEG, E. A monte carlo study of dislocation growth and etching of crystals. *Journal of Crystal Growth 219*, 1-2 (2000), 165–175.

[25] DAS, A., AND MITTEMEMEIJER. A monte carlo simulation of solidification structures of binary alloys. *Philosophical Magazine A 81*, 11 (2001), 2725–2742.

[26] DASH, W. Copper precipitation on dislocations in silicon. *Journal of Applied Physics 27*, 10 (1956), 1193–1415.

[27] DE LEEUW, N. H., PARKER, S. C., AND HARDING, J. H. Molecular dynamics simulation of crystal dissolution from calcite steps. *Physical Review B 60*, 19 (November 1999), 13792–13799.

[28] DITCHEK, B. M., HEFTER, J., MIDDLETON, T. R., AND PELLEG, J. Mircostructure of czochralski-grown si-tasi$_2$ eutectic composites. *Journal of Crystal Growth 102* (1990), 401–412.

[29] DITCHEK, B. M., YACOBI, B. G., AND LEVINSON, M. Depletion zone limited transport in si-tasi$_2$ eutectic composites. *Journal of Applied Physics 63*, 6 (March 15 1988), 1964–1970.

[30] DREVET, B., GARANDET, J. P., CAMEL, D., AND FAVIER, J. J. Influence of thermal buoyancy on fibrous eutectic growth i. seregation results in the sn-cu_6sn_5 system. *Journal of Crystal Growth 129* (1993), 549–558.

[31] DROLET, F., ELDER, K. R., GRANT, M., AND KOSTERLITZ, J. M. Phase-field modeling of eutectic growth. *Physical Review E 61*, 6 (June 2000), 6705–6720.

[32] ELWENSPOEK, E. Comment on the α-factor of jackson for crystal growth from solution. *Journal of Crystal Growth 78* (1986), 353–356.

[33] ENCKEVORT, W. J. P. V., AND EERDEN, J. P. Monte carlo simulation of a $\{111\}$ diamond face around the roughening transition. *Journal of Crystal Growth 47* (1979), 501–508.

[34] ENCKEVORT, W. J. P. V., AND SMET, F. Dislocation etching of rough crystal faces. *Journal of Crystal Growth 89* (1988), 471–477.

[35] FISHER, D. J., AND KURZ, W. A theory of branching limited growth of irregular eutectics. *Acta Metallurgica 28*, 6 (1980), 777–794.

[36] FRANK, F. C. Capillary equilbria of dislocated crystals. *Acta Crystallographica 4*, 6 (November 1951), 497–501.

[37] GILMER, G. Ising model simulations of impurity trapping in silicon. *Materials Research Society Symposium Proceedings 13* (1983), 249–261.

[38] GILMER, G. H. Growth on imperfect crystal faces. *Journal of Crystal Growth 35* (1976), 15–28.

[39] GILMER, G. H. *Chemistry and Physics of Solid Surfaces*, vol. 5. Springer-Verlag, Heidelberg, Germany, 1984, ch. Ising Model Simulations of Crystal Growth, pp. 297–316.

[40] GILMER, G. H., AND BROUGHTON, J. Q. Computer modeling of mass transport along surfaces. *Annual Reviews - Materials Science 16* (1986), 487–516.

[41] GILMER, G. H., AND JACKSON, K. A. *Crystal Growth and Materials*. North-Holland Publishing Company, 1977, ch. Computer Simulation of Crystal Growth, pp. 80–114.

[42] GUANG-ZHAO, L., EERDEN, J. P. V. D., AND BENNEMA, P. The opening and closing of a hollow dislocation core: A monte carlo simulation. *Journal of Crystal Growth 58* (1982), 152–162.

[43] HUNT, J. D. Developments in eutectics. *Journal of Crystal Growth 3, 4* (1968), 82–91.

[44] HUNT, J. D. Pattern formation in solidification. *Science and Technology of Advanced Materials 2* (2001), 147–155.

[45] HUNT, J. D., AND JACKSON, K. A. Binary eutectic solidification. *Transactions of the Metallurgical Society of Aime 236*, 6 (1966), 843–852.

[46] HUNT, J. D., AND JACKSON, K. A. The dendrite-eutectic transition. *Transactions of the Metallurgical Society of AIME 239* (June 1967), 864–867.

[47] ISING, E. Beitrag zur theorie des ferromagnetismus. *Zeitschrift Für Physik 31* (February 1925), 253–258.

[48] ISRAELACHVILI, J. *Intermolecular and Surface Forces*, 2nd ed. Academic Press, 1997, ch. 10.

[49] JACKSON, K. On the theory of crystal growth: the fundamental rate equation. *Journal of Crystal Growth 5* (1969), 13–18.

[50] JACKSON, K. Solidification structures of pure metals. In *Metallography, Structures and Phase Diagrams*, M. B. Bever, Ed., 8 ed., vol. 8 of *Metals Handbook*. American Society for Metals, Metals Park, Ohio, 1973, pp. 147–149.

[51] JACKSON, K. A. Interface structure. In *Growth and Perfection of Crystals* (Cooperstown, New York, August 1958), R. H. Doremus, B. W. Roberts, and D. Turnbull, Eds., John Wiley and Sons, pp. 319–324.

[52] JACKSON, K. A. Kinetics of alloy soldification. *Canadian Journal of Physics 36* (1958), 683–691.

[53] JACKSON, K. A. Mechanism of growth. In *Liquid Metals and Solidification* (Chicago, November, 1957 1958), The American Society for Metals, America Society for Metals, pp. 174–186.

[54] JACKSON, K. A. Computer modeling of atomic scale crystal growth processes. *Journal of Crystal Growth 198*, 199 (1999), 1–9.

[55] JACKSON, K. A., BEATTY, K. M., AND MINKE, M. V. Monte carlo simulation of non-equilibrium segregation during crystal growth. *Journal of Non-Crystalline Solids 219* (1997), 100–109.

[56] JACKSON, K. A., CHADWICK, G. A., AND KLUGERT, A. Lamellar growth: an electric analog. *Transactions of the Metallugical Society of AIME 230* (December 1964), 1547–1553.

[57] JACKSON, K. A., AND CHALMERS. Kinetics of solidification. *Canadian Journal of Physics 34* (1956), 473–490.

[58] JACKSON, K. A., GILMER, G. H., AND TEMKIN, D. E. Monte carlo simulations of the rapid crystallization of bismuth-doped silicon. *Physical Review Letters 75*, 13 (September 1995), 2530–2533.

[59] JACKSON, K. A., GILMER, G. H., TEMKIN, D. E., AND BEATTY, K. M. Microsegregation far from equilibrium. *Journal of Crystal Growth 163* (1996), 461–469.

[60] JACKSON, K. A., AND HUNT, J. D. Lamellar and rod eutectic growth. *Transactions of the Metallurgical Society of Aime 236*, 8 (1966), 1129–1142.

[61] KARAN, S., GUPTA, S., AND GUPTA, S. P. Revelation of dislocation etch pits in mixed crystals of ammonium-potassium sulphate, $[k_{1-x}(nh_4)_x]_2so_4$. *Journal of Crystal Growth 233* (2001), 555–560.

[62] KARMA, A. Beyond steady-state lamellar eutectic growth. *Physical Review Letters 59*, 1 (July, 6 1987), 71–74.

[63] KARMA, A. Phase-field model of eutectic growth. *Physical Review E 49*, 3 (March 1994), 2245–2250.

[64] KARMA, A., AND J., R. W. Phase-field method for computationally efficient modeling of solidification with arbitrary interface kinetics. *Physical Review E 53*, 4 (April 1996), R3017–R3020.

[65] KOSTERLITZ, J. M., AND THOULESS, D. J. Ordering, metastability and phase transitions in two-dimensional systems. *Journal of Physics C: Solid State Physics 6* (1973), 1181–1203.

[66] KOTRLA, M. Numerical simulations in the theory of crystal growth. *Computer Physics Communications 97* (1996), 82–100.

[67] KRUSE, R. L., LEUNG, B. P., AND TONDO, C. L. *Data Structures and Program Design in C.* Prentice Hall, 1991, ch. Binary Trees, pp. 59–97.

[68] KURZ, W., AND TRIVEDI, R. Solidification microstructures: Recent developments and future directions. *Acta Metallurgica et Materialia 38*, 1 (1990), 1–17.

[69] LAUDISE, R. A., CARRUTHERS, J. R., AND JACKSON, K. A. Crystal growth. *Annual Review of Materials Science 1* (1971), 253–288.

[70] LEAMY, H. J., AND GILMER, G. H. The equilibrium properties of crystal surface steps. *Journal of Crystal Growth 24/25* (1974), 499–502.

[71] LEAMY, H. J., AND JACKSON, K. A. Roughness of the crystal-vapor interface. *Journal of Applied Physics 42*, 5 (1971), 2121–2127.

[72] LOVELL, L. C., VOGEL, F. L., AND WERNICK, J. H. Etching reagents for dislocations in metal crystals. *Metal Progress 75*, 5 (1958), 96.

[73] LUI, J. M., WU, Z. C., AND LIU, Z. G. Monte-carlo simulation of directional growth of lamellar eutectic. *Scripta Meterialia 38*, 5 (1998), 715–722.

[74] MAGNIN, P., AND KURZ, W. An analytical model of irregular eutectic growth and its application to fe-c. *Acta Metallurgica 35*, 5 (1987), 1119–1128.

[75] MAGNIN, P., MASON, J., AND TRIVEDI, R. Growth of irregular eutectics and the al-si system. *Acta Metallurgica et Materialia 39*, 4 (1991), 469–480.

[76] MATSUMOTO, M., AND NISHIMURA, T. Mersenne twister: a 623-dimensionally equidistributed uniform pseudo-random number generator. *ACM Transactions on Modeling and Computer Simulation 8*, 1 (1998), 3–30.

[77] MERRITT, E. A., AND BACON, D. J. Raster3d: Photorealistic molecular graphics. *Methods in Enzymology 277* (1997), 505–525.

[78] MUKERJI, S., AND KAR, T. Etch pit study of different crystallographic faces of l-arginine hydrobromide monohydrate (lahbr) in alcohols. *Journal of Crystal Growth 200* (1999), 543–549.

[79] NABARRO, F., AND NUNES, R. *Theory of Crystal Dislocations.* International series of monographs on physics. Clarendon P., Oxford,, 1967.

[80] NEUMANN, H. B., SCHNEIDER, J. R., Sü β ENBACH, STOCK, S. R., AND REK, Z. U. Si-tasi$_2$ in situ composites: a new monochromator material for hard x-rays. *Nuclear Instruments and Methods in Physics Research A 372* (1996), 551–555.

[81] ONSAGER, L. Reciprocal relations in irreversible processes. ii. *Physical Review 38* (December 1931), 2265–2279.

[82] ONSAGER, L. Crystal statistics. i. a two-dimensional model with an order-disorder transition. *Physical Review 65*, 4 (February 1944), 117–149.

[83] PARK, N.-S., MYOUNG-WON, K., LANGFORD, S. C., AND DICKINSON, J. T. Atomic layer wear of single-crystal calcite in aqueous solution using scanning force microscopy. *Journal of Applied Physics 80*, 5 (2002), 2680–2686.

[84] PIRICH, R. G. Gravitational induced convection during directional solidification of off-eutectic mn-bi alloys. In *Materials Processing in Reduced Gravity Environment of Space*, G. E. Rindone, Ed. North Holland, New York, 1982, pp. 593–602.

[85] PIRICH, R. G., AND LARSON, D. J. Influence of gravity driven convection on the directional solidification of bi/mnbi eutectic composites. In *Materials Processing in Reduced Gravity Environment of Space*, G. Rindone, Ed. North Holland, New York, 1982, pp. 523–531.

[86] POPOV, D. I., REGEL, L. L., AND WILCOX, W. R. One-dimensional phase-field model for binary alloys. *Journal of Crystal Growth 212* (2000), 574–583.

[87] PRESS, W. H., TEUKOLSKY, S. A., VETTERLING, W. T., AND FLANNERY, B. P. *Numerical Recipes in C*, 2nd ed. Cambridge University Press, 1994, ch. Chapter 9. Root Finding and Nonlinear Sets of Equations, pp. 347–393.

[88] QUENISSET, J. M., SOKOLOWSKI, R., AND GLICKSMAN, M. E. Effects of forced convection flow on directional solidification of pd-sn and cd-zn eutectic alloys. *Journal of Crystal Growth 63* (1983), 389–399.

[89] SAMALAM, V. K. Si-tasi$_2$ eutectic composites as an example of percolation system. *Journal of Applied Physics 67*, 4 (February 15 1990), 2165–2167.

[90] SETH, J., AND WILCOX, W. R. Effect of convection on the mircostructure of lamellar eutectic growing with a stepped interface. *Journal of Crystal Growth 114* (1991), 357–363.

[91] SHIM, Y., LANDAU, D. P., AND PAL, S. Kinetic monte carlo simulations of binary alloy film growth. *Journal of Physics: Condensenced Matter 11* (1999), 10007–10018.

[92] SHUGARD, W. J., WEEKS, J. D., AND GILMER, G. H. Monte carlo test of theories for the planar model, the f model, and related systems. *Physical Review Letters 41*, 20 (Nov 1978), 1399–1402.

[93] SINGH, R. K., AND BAJAJ, R. Advances in chemical-mechanical planarization. *MRS Bulletin 27*, 10 (October 2002), 743–747.

[94] SUNAGAWA, I., AND BENNEMA, P. Observations of the influence of stress fields on the shape of growth and dissolution spirals. *Journal of Crystal Growth 53* (1981), 490–504.

[95] SWENDSEN:1976. Thermodynamic properties of surface steps. *Journal of Crystal Growth 36* (1976), 11–14.

[96] VEENENDAAL, V. E., BEURDEN, V. P., ENCKEVORT, V. W. J. P., VLIEG, E., SUCHTELEN, V. J., AND ELWENSPOEK, M. Monte carlo study of kinetic smoothing durring dissolution and etching of kossel(100) and silicon (111) surfaces. *Journal of Applied Physics 88*, 8 (15 October 2000), 4595–4604.

[97] WADLEY, H. N. G., ZHOU, X., JOHNSON, R. A., AND NEUROCK, M. Mechanisms, models and methods of vapor deposition. *Progress in Materials Science 46* (2001), 329–377.

[98] WEEKS, J. D., AND GILMER, G. H. Thermodynamic properties of surface steps. *Journal of Crystal Growth 43* (1978), 385–387.

[99] WILSON, H. A. On the velocity of solidification of supercooled liquids. *Philosophical Magazine and Journal of Science 50*, 303 (1900), 238–250.

[100] WOLCZYNSKI, W. Thermodynamics of irregular eutectic growth. *Materials Science Forum 215-216* (1996), 303–312.

[101] WOODRASKA, D., AND JASZCZAK, J. A monte carlo simulation method for {111} surfaces of silicon and other diamond-cubic materials. *Surface Science 374*, 1-3 (1997), 319–32.

[102] WOODRASKA, D. L., AND JASZCZAK, J. A. Roughening and preroughening of diamond-cubic 111 surfaces. *Physical Review Letters 78*, 2 (1997), 258–61.

[103] XIAO, R., ALEXANDER, J. I., AND ROSENBERGER, F. Growth morphologies of crystal surfaces. *Physical Review A 43*, 6 (March 1991), 2977–2992.

[104] XIAO, R., ALEXANDER, J. I. D., AND ROSENBERGER, F. Microscopic-growth morphologies in binary systems. *Physical Review A 45*, 2 (1992), R571–574.

[105] XIAO, R., ALEXANDER, J. I. D., AND ROSENBERGER, F. Eutectic and off-eutectic growth patterns. *Materials Science and Engineering A178* (1994), 233–238.

[106] ZHU, M. F., AND HONG, C. P. Modeling of microstructure evolution in regular eutectic growth. *Physical Review B 66* (2002), 155428.